

Online Adaptive Real-Time Beamforming Design for Dynamic Environments in Cell-Free Systems

Guanghai Chen, *Graduate Student Member, IEEE*, Zheng Wang, *Senior Member, IEEE*, Hongxin Lin, Pengguang Du, *Graduate Student Member, IEEE*, Yongming Huang, *Fellow, IEEE*

Abstract—In this paper, we consider real-time beamforming design for dynamic wireless environments with varying channels and different numbers of access points (APs) and users in cell-free systems. Specifically, a sum spectral efficiency (SE) maximization optimization problem is formulated for the beamforming design in dynamic wireless environments of cell-free systems. To efficiently solve it, a high-generalization network (HGNet) is proposed to adapt to the changing numbers of APs and users. Then, a high-generalization beamforming module is also designed in HGNet to extract the valuable features for the varying channels, and we theoretically prove that such a high-generalization beamforming module is able to reduce the upper bound of the generalization error. Subsequently, by online adaptively updating about 3% of the parameters of HGNet, an online adaptive updating (OAU) algorithm is proposed to enable the online adaptive real-time beamforming design for improving the sum SE. Numerical results demonstrate that the proposed HGNet with OAU algorithm achieves a higher sum SE with a lower computational cost on the order of milliseconds.

Index Terms—Cell-free systems, beamforming, real-time, deep learning, generalization, dynamic wireless environments.

I. INTRODUCTION

RECENTLY, cell-free systems have received considerable attentions [2], [3]. By connecting all access points (APs) to a central processing unit (CPU) via backhaul links, cell-free systems allow multiple APs to collaboratively design beamforming to serve users within the network coverage area, thus eliminating many interference issues present in cellular systems [4], [5]. Nevertheless, beamforming design is a nonconvex optimization problem that is difficult to solve efficiently [6], [7]. Conventional optimization algorithms like the weighted minimum mean square error (WMMSE) algorithm [8] usually use the convex approximation to obtain a stable solution of the beamforming design. Unfortunately, most of

them require multiple iterations and matrix inversions, which are difficult to meet the demands of the real-time beamforming design.

To facilitate the real-time implementation, deep learning has been extensively applied to the beamforming design of cell-free systems [9], [10]. Notably, by applying graph neural networks (GNNs), the work in [11] proposed an Edge-GNN to solve the sum spectral efficiency (SE) maximization problem of cooperative beamforming design. Based on the weight sharing mechanism of convolutional neural networks (CNNs), Ref. [12] designed a SUNet with high computational efficiency for achieving the beamforming design in cell-free systems. Once trained, these deep learning algorithms require only simple feed-forward computations to infer beamforming, enhancing the real-time reflection speed compared to WMMSE algorithm. However, these methods generally assume to work in a fixed configuration, i.e., the channel conditions are the same for the training and the inference phases.

In practice, communication systems normally operate in dynamic wireless environments due to user mobility and random distributions for various transmission media [13]. Given these realistically dynamic wireless environments, most deep learning-based beamforming design algorithms struggle to achieve good performance under real-time requirements. This is since the varying channels resulting from dynamic wireless environments cause the data distribution fed into deep learning to be different in the training and the inference phases. Such shift violates the basic assumptions of deep learning, i.e., the same data distribution in the training and the inference stages can yield better generalization performance [14]. Although retraining the model with current channel data can improve the generalization of varying channels, it is time-consuming and insufficient for real-time applications.

There have been some pioneering works utilizing deep learning to consider dynamic wireless environments, where the channels vary over periods while remaining constant within each period [15], [16], [17]. Specifically, by using continuous learning to adapt to a new period without forgetting the knowledge learned from previous ones, [15] optimized power allocation for dynamic wireless environments in single-input single-output (SISO) cellular systems. The work in [16] proposed a meta-gating framework including outer and inner networks to realize the beamforming design for dynamic wireless environments in multiple-input single-output (MISO) cellular systems. The outer network evaluated the importance of the inner network's parameters under varying channels, and then decided which subset of the inner network should be

This work was supported by the National Natural Science Foundation of China under Grants 62225107 and 62371124, the Fundamental Research Funds for the Central Universities under Grant 2242022k60002, the Jiangsu Provincial Scientific Research Center of Applied Mathematics under Grant BK20233002, and the Postgraduate Research & Practice Innovation Program of Jiangsu Province under Grant KYCX23_0259. This paper was partially presented at the 2025 IEEE Wireless Communications and Networking Conference (WCNC) [1]. (Corresponding authors: Yongming Huang, Zheng Wang and Hongxin Lin.)

G. Chen, Z. Wang, P. Du and Y. Huang are with the School of Information Science and Engineering, and the National Mobile Communications Research Laboratory, Southeast University, Nanjing 210096, China; G. Chen and Y. Huang are also with the Pervasive Communications Center, Purple Mountain Laboratories, Nanjing 211111, China. (e-mail: cgh@seu.edu.cn, wznuaa@gmail.com, pgdu@seu.edu.cn, huangym@seu.edu.cn).

H. Lin is with the Purple Mountain Laboratories, Nanjing 211111, China. (email: lnhongxin@pmlabs.com.cn).

activated through a gating operation. For intelligent omnidirectional surface assisted MISO cellular systems, [17] proposed a meta-critic reinforcement learning capable of recognizing changes in dynamic wireless environments and automatically performing the self-renewal of the learning mode, while the beamforming design was performed by the low-performance zero-forcing.

Although the above methods have been applied to dynamic wireless environments, it is still a challenge to apply them to the real-time beamforming design for dynamic wireless environments in cell-free systems. The reasons are as follows. Firstly, compared to SISO and MISO cellular systems, the multiple-input multiple-output (MIMO) cell-free systems considered in this paper contain numerous APs and users with multiple antennas, which greatly hinders the application of these methods for the real-time beamforming design. Secondly, compared to the power allocation in [15] and the zero-forcing in [17], the number of the optimized variables for the beamforming design is considerably higher, further increasing the challenge of the real-time beamforming design. Thirdly, dynamic wireless environments potentially lead to a variation in the association relationship between APs and users for cell-free systems, i.e., the number of APs and users changes over periods while remaining constant within each period. The algorithms in [15], [16], [17] probably need to retrain the network architectures and parameters as the number of users and APs varies in cell-free systems, which is also difficult to meet real-time requirements.

Motivated by the above challenges, this paper investigates the real-time beamforming design for dynamic wireless environments in cell-free systems. The objective is to maximize the sum SE while maintaining computational efficiency for the varying channels with the different numbers of APs and users. To achieve the objective, this paper proposes a high-generalization network (HGNet) with an online adaptive updating (OAU) algorithm. More specifically, the major contributions are summarized as follows:

- 1) To effectively characterize the dynamic wireless environments in cell-free systems, the channels as well as the number of APs and users are modeled as varying over periods and remaining constant within each period. Meanwhile, a sum SE maximization optimization problem for the varying channels and the different numbers of APs and users is built for the beamforming design in dynamic wireless environments of cell-free systems.
- 2) To solve the non-convex optimization problem, we propose HGNet. Particularly, HGNet incorporates the residual structure of CNNs to map channel state information (CSI) to beamforming with high computational efficiency, which also adapts to the varying numbers of APs and users. HGNet also designs a high-generalization beamforming module to extract the valuable features for the varying channels, and we theoretically prove that the high-generalization beamforming module decreases the upper bound of the generalization error. This helps HGNet to yield a better generalization sum SE for dynamic wireless environments.

- 3) To enable the online adaptive real-time beamforming design, an OAU algorithm is proposed to adaptively update about 3% of the parameters of HGNet online, taking a computationally efficient information entropy as the loss function. This further enhances the sum SE performance of dynamic wireless environments with the varying channels and the different numbers of APs and users in cell-free systems.
- 4) Numerical results are conducted to validate the effectiveness of the proposed HGNet with OAU algorithm. For the varying channels and the different numbers of APs and users, the average sum SE performance of HGNet outperforms those of the recent deep learning algorithms Edge-GNN [11] and SUNet [12], where the average computational cost of HGNet is also the lowest on the millisecond scale. Meanwhile, the proposed OAU algorithm further improves the sum SE performance of HGNet with an average computation cost in the order of milliseconds.

The rest of this paper is organized as follows. In Section II, the system model is introduced, followed by formulating a sum SE maximization optimization problem with the varying channels and the different numbers of APs and users. In Section III, the HGNet containing the high-generalization beamforming module is proposed, and a theoretical proof that the high-generalization beamforming module can reduce the upper bound of the generalization error is given. In Section IV, the OAU algorithm is proposed to online adaptively update the parameters of HGNet to realize the online adaptive real-time beamforming design with increasing sum SE performance. In Section V, some experimental results for HGNet and OAU algorithm are showed and analyzed. Finally, some conclusions are provided in Section VI.

Notations: The scalar, vector, and matrix are denoted by lowercase letter x , boldface lowercase letter \mathbf{x} , and boldface uppercase letter \mathbf{X} , respectively. \mathbb{C} and \mathbb{R} denote the sets of complex and real numbers, respectively. $(\cdot)^H$ denotes the conjugate transpose. $(\cdot)^{-1}$ denotes the matrix inversion. $\{\cdot\}$ denotes the set. \sup denotes the minimum upper bound.

II. SYSTEM MODEL

As illustrated in Fig.1, a dynamic wireless environment for cell-free systems is considered, where the channels as well as the number of APs and users vary between periods and remain constant within each period. Scenarios with the considered dynamic environment can be widely found in practice. For instance, autonomous vehicles move from high-density areas to open environments, the channel changes accordingly from Rayleigh fading with non-line-of-sight (NLoS) to Rician fading with LoS [18]. To ensure the safety of autonomous vehicles, real-time communication is crucial [19], often requiring resource allocation at the millisecond level to support low-latency communication [20]. In such cases, the period can be defined based on environmental conditions, such as “time in high-density areas” or “time in open environments”. Further, let $\mathcal{T} = \{1, \dots, T\}$ denote the set of periods, where I_t users are assumed to access Q_t APs in the t^{th}

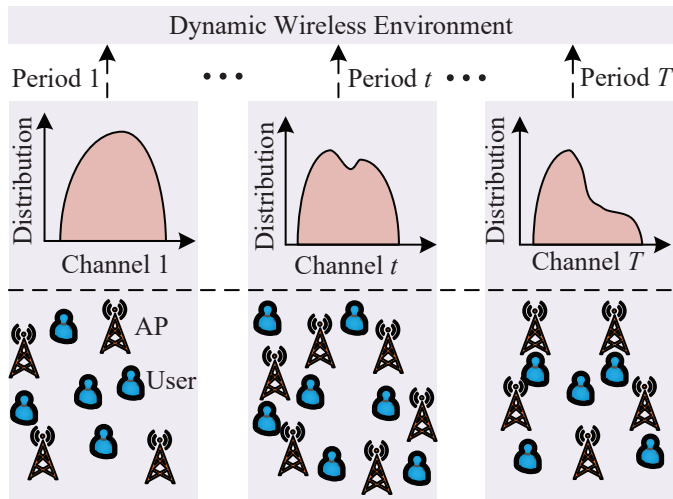


Fig. 1: An illustration for dynamic wireless environments with the varying channels and the different numbers of APs and users.

period. $\mathcal{Q}_t = \{1_t, \dots, Q_t\}$ and $\mathcal{I}_t = \{1_t, \dots, I_t\}$ denote the sets of APs and users at the t^{th} period. Each AP is equipped with M antennas, and each user with N antennas. All APs are connected to a CPU via backhaul links for exchanging information, where the CPU can access global CSI to collaboratively design beamforming for improving the system sum SE¹ [12], [22]. To simplify the notation, i and j denote the indexes of users, and q denotes the index of AP. The received signal of the i^{th} user at the t^{th} period is represented as

$$\mathbf{y}_{i,t} = \mathbf{H}_{i,t} \mathbf{v}_{i,t} s_{i,t} + \sum_{j \neq i} \mathbf{H}_{i,t} \mathbf{v}_{j,t} s_{j,t} + \mathbf{z}_{i,t} \in \mathbb{C}^{N \times 1}, \quad (1)$$

where $\mathbf{H}_{i,t} \in \mathbb{C}^{N \times Q_t M}$ and $\mathbf{v}_{i,t} \in \mathbb{C}^{Q_t M \times 1}$ denote the CSI matrix and beamforming vector of the AP set \mathcal{Q}_t to the i^{th} user at the t^{th} period. $s_{i,t}$ denotes the data sent to the i^{th} user at the t^{th} period. $\mathbf{z}_{i,t} \sim \mathcal{CN}(\mathbf{0}, \sigma_{i,t}^2 \mathbf{I})$ denotes the additive noise. From Eq.(1), the SE of the i^{th} user at the t^{th} period is denoted as

$$R_{i,t} = \log \left| \mathbf{I} + \mathbf{H}_{i,t} \mathbf{v}_{i,t} \mathbf{v}_{i,t}^H \mathbf{H}_{i,t}^H \left(\sum_{j \neq i} \mathbf{H}_{i,t} \mathbf{v}_{j,t} \mathbf{v}_{j,t}^H \mathbf{H}_{i,t}^H + \sigma_{i,t}^2 \mathbf{I} \right)^{-1} \right|. \quad (2)$$

To better depict the influence brought by dynamic wireless environments, we consider the sum SE maximization problem

¹This paper focuses on the real-time beamforming design under dynamic wireless environments with varying channels and different numbers of APs and users in cell-free systems, assuming that all APs in the network coverage area serve all users simultaneously. This assumption actually reduces the scalability of cell-free systems [21]. However, when user scheduling techniques are implemented to improve the scalability of cell-free systems, the proposed method is still able to perform despite the varying number of users caused by the user scheduling techniques. This is because the proposed method is based on the convolution operation, which guarantees that the dimension of the output varies flexibly with that of the input. Therefore, in the future, we will integrate a deep learning-based user scheduling algorithm into the proposed method to further improve the scalability of cell-free systems.

for the varying channels and the different numbers of APs and users in cell-free systems, i.e.,

$$\begin{aligned} \max_{\mathbf{v}_{i,t}} \quad & \sum_{i=1}^{I_t} R_{i,t} \\ \text{s.t.} \quad & \sum_{i=1}^{I_t} \mathbf{v}_{i,t}^{q,H} \mathbf{v}_{i,t}^q \leq P_{\max}, \forall q \in \mathcal{Q}_t, \forall t \in \mathcal{T}, \\ & D(\mathbf{H}_t) \Leftarrow t, \forall t \in \mathcal{T}, \\ & (Q_t, I_t) \Leftarrow t, \forall t \in \mathcal{T}, \end{aligned} \quad (3)$$

where P_{\max} is the maximum transmit power of the AP. $\mathbf{v}_{i,t}^q \in \mathbb{C}^{M \times 1}$ is the beamforming vector of the q^{th} AP to the i^{th} user at the t^{th} period, and $\mathbf{v}_{i,t} = [\mathbf{v}_{i,t}^{1,H}, \dots, \mathbf{v}_{i,t}^{q,H}, \dots, \mathbf{v}_{i,t}^{Q_t,H}] \in \mathbb{C}^{Q_t M \times 1}$. $\mathbf{H}_t = [\mathbf{H}_{1,t}^H, \dots, \mathbf{H}_{i,t}^H, \dots, \mathbf{H}_{I_t,t}^H]^H \in \mathbb{C}^{I_t N \times Q_t M}$ denotes the CSI matrix of the AP set \mathcal{Q}_t to the user set \mathcal{I}_t at the t^{th} period. $D(\mathbf{H}_t)$ denotes the distribution of \mathbf{H}_t .

Remark 1: The constraint $D(\mathbf{H}_t) \Leftarrow t, \forall t \in \mathcal{T}$ in the optimization problem (3) indicates the channels varying with the period t for dynamic wireless environments in cell-free systems. Due to the variations in the channels, the input CSI of deep learning has different distributions during the training and the inference phases. This violates the underlying assumption of deep learning that better generalization performance is only produced by using the same data distribution in the training and the inference stages. As a result, the constraint $D(\mathbf{H}_t) \Leftarrow t, \forall t \in \mathcal{T}$ severely increases the difficulty of solving the optimization problem (3) leveraging deep learning.

Remark 2: The constraint $(Q_t, I_t) \Leftarrow t, \forall t \in \mathcal{T}$ in the optimization problem (3) describes the number of APs and users varying with the period t for dynamic wireless environments in cell-free systems. The changing numbers of APs and users result in a variation in the dimension of the input CSI for deep learning, requiring the corresponding dimension of the output beamforming to adjust accordingly. In other words, the constraint $(Q_t, I_t) \Leftarrow t, \forall t \in \mathcal{T}$ requires that the dimension of the output beamforming of deep learning flexibly varies with that of the input CSI. This may require deep learning method to retrain the network architectures and parameters in a remarkably time-consuming manner, which fails to meet the demands of the real-time beamforming design.

Note that the optimization problem (3) is non-convex, which can be solved approximately by traditional optimization algorithms with high computational complexity. However, it is difficult to realize the real-time beamforming design. Deep learning is a good alternative to improve the computational efficiency. Unfortunately, according to *Remark 1* and *Remark 2*, applying deep learning to solve the optimization problem (3) is also a challenge in terms of generalization and real-time performance due to the constraints $D(\mathbf{H}_t) \Leftarrow t, \forall t \in \mathcal{T}$ and $(Q_t, I_t) \Leftarrow t, \forall t \in \mathcal{T}$. As a result, it is necessary to carry out a high-generalization real-time beamforming design for dynamic wireless environments with the varying channels and the different numbers of APs and users in cell-free systems.

III. PROPOSED HGNET

In this section, we pay our attention on designing a HGNet to implement the high-generalization real-time beamforming

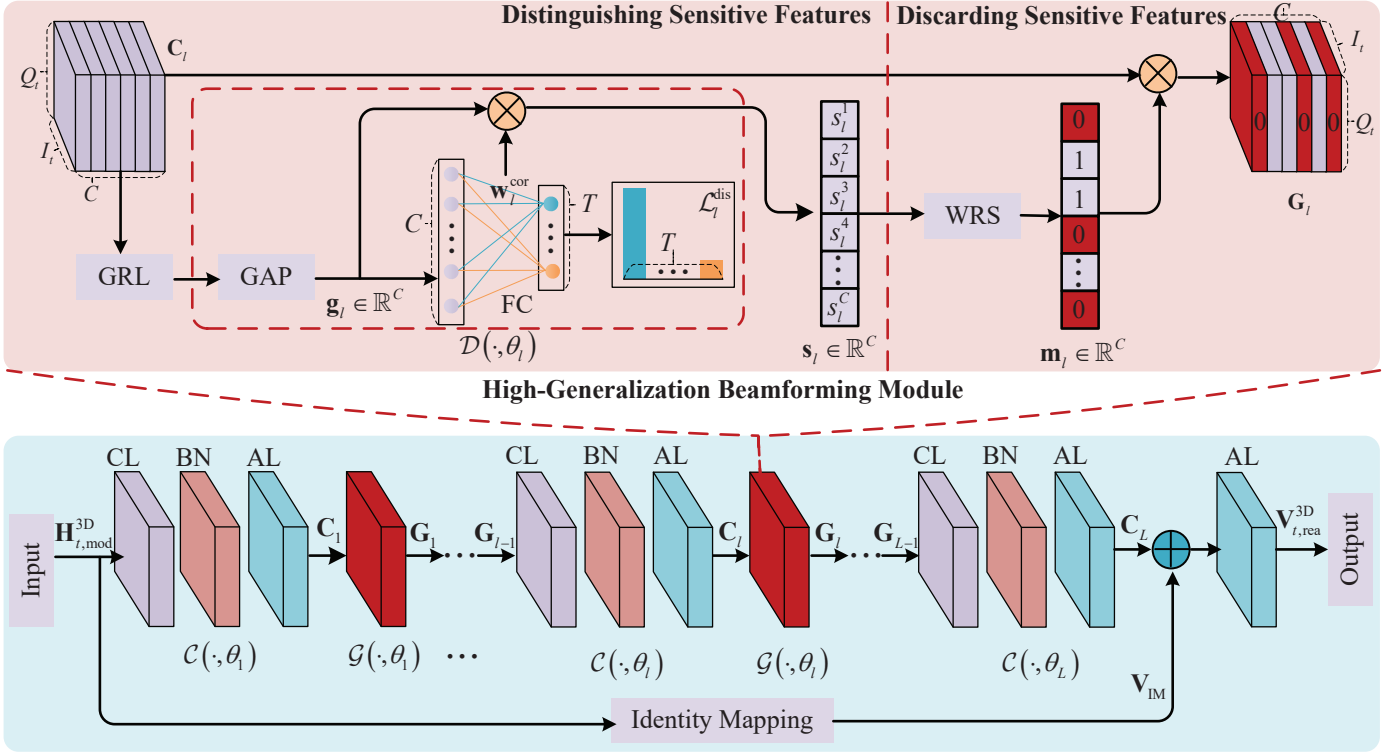


Fig. 2: Proposed HGNet.

design for dynamic wireless environments with the varying channels and the different numbers of APs and users in cell-free systems by solving the optimization problem (3). As illustrated in Fig.2, the proposed HGNet mainly includes an input module, a convolution unit $\mathcal{C}(\cdot, \theta_t)$, a high-generalization beamforming module $\mathcal{G}(\cdot, \theta_t)$ and an output module. Specifically, the input module transforms a complex-valued CSI into a real-valued CSI. $\mathcal{C}(\cdot, \theta_t)$ maps the real-valued CSI to beamforming with low computational complexity and satisfying $(Q_t, I_t) \Leftarrow t, \forall t \in \mathcal{T}$ in the optimization problem (3). Subsequently, $\mathcal{G}(\cdot, \theta_t)$ is specially designed to improve the sum SE performance for $D(\mathbf{H}_t) \Leftarrow t, \forall t \in \mathcal{T}$ in the optimization problem (3). Finally, the output module yields the complex-valued beamforming that satisfies the power constraint.

A. Input

Since deep learning methods such as CNNs normally deal with three-dimensional (3D) real numbers, the input module converts $\mathbf{H}_t \in \mathbb{C}^{I_t N \times Q_t M}$ into a 3D real-valued CSI tensor $\mathbf{H}_{t,\text{mod}}^{3D} \in \mathbb{R}^{Q_t \times I_t \times MN}$ by computing modulus values and dimension transformations. ²

B. Convolution Unit $\mathcal{C}(\cdot, \theta_t)$

$\mathcal{C}(\cdot, \theta_t)$ aims to achieve the mapping from $\mathbf{H}_{t,\text{mod}}^{3D} \in \mathbb{R}^{Q_t \times I_t \times MN}$ to beamforming with fulfilling $(Q_t, I_t) \Leftarrow t, \forall t \in \mathcal{T}$ in the optimization problem (3). Particularly, $(Q_t, I_t) \Leftarrow t, \forall t \in \mathcal{T}$ requires that the dimension

²In this paper, the first, second and third dimensions of a 3D tensor are denoted as width, height and third dimension, respectively.

of the output beamforming of deep learning should flexibly change with the dimension of the input $\mathbf{H}_{t,\text{mod}}^{3D} \in \mathbb{R}^{Q_t \times I_t \times MN}$. Fortunately, the output dimension of the convolution unit is determined by the input data dimension and the convolutional architectural parameters. Accordingly, it is encouraged to apply the convolution unit to derive some architectural conditions for satisfying $(Q_t, I_t) \Leftarrow t, \forall t \in \mathcal{T}$. On the other hand, the unique weight sharing mechanism of the convolution unit significantly reduces the computational complexity of neural networks, which is also in line with the goal of the real-time beamforming design. Consequently, $\mathcal{C}(\cdot, \theta_t)$ selects the convolution unit to cascade into a deep structure with L layers, where each layer contains a convolution layer (CL), a batch normalization (BN) layer, and an activation layer (AL). Formally, the formula of the l^{th} layer $\mathcal{C}(\cdot, \theta_t)$ is defined as

$$\mathbf{C}_l = \text{AL}(\text{BN}(\text{CL}(\mathbf{G}_{l-1}, \theta_t))), \quad (4)$$

where \mathbf{C}_l denotes the output of $\mathcal{C}(\cdot, \theta_t)$, and θ_t is the parameters of HGNet. \mathbf{G}_{l-1} denotes the input of $\mathcal{C}(\cdot, \theta_t)$, and $\mathbf{G}_0 = \mathbf{H}_{t,\text{mod}}^{3D} \in \mathbb{R}^{Q_t \times I_t \times MN}$. $\text{CL}(\cdot, \cdot)$ denotes the convolution operation. $\text{BN}(\cdot)$ denotes the BN operation, which is added after the CL for reducing the overfitting probability [23]. $\text{AL}(\cdot)$ denotes the AL operation [24], which selects the commonly used $\text{ReLU}(x) = \max(0, x)$. Note that the last layer $\mathcal{C}(\cdot, \theta_L)$ outputs the real and imaginary parts of beamforming, which should contain both positive and negative values. Thus, $\text{AL}(\cdot)$ in $\mathcal{C}(\cdot, \theta_L)$ can adopt $\text{Tanh}(x) = \frac{e^x - e^{-x}}{e^x + e^{-x}}$.

Remark 3: For the constraint $(Q_t, I_t) \Leftarrow t, \forall t \in \mathcal{T}$ in the optimization problem (3), when the dimension of the input 3D real-valued CSI $\mathbf{H}_{t,\text{mod}}^{3D}$ at the t^{th} period is $Q_t \times I_t \times MN$, the dimension of the corresponding output beamforming should be

a 3D complex-valued tensor of dimension $Q_t \times I_t \times M$, which can be transformed into a 3D real-valued tensor of dimension $Q_t \times I_t \times 2M$. At the t^{th} period, the dimension of the input 3D real-valued CSI $\mathbf{H}_{t,\text{mod}}^{\text{3D}}$ changes from $Q_t \times I_t \times MN$ to $Q_{t'} \times I_{t'} \times MN$, then the dimension of the corresponding output beamforming should vary from $Q_t \times I_t \times 2M$ to $Q_{t'} \times I_{t'} \times 2M$.

Based on Remark 3, when $\mathbf{H}_{t,\text{mod}}^{\text{3D}} \in \mathbb{R}^{Q_t \times I_t \times MN}$ is inputted to $\mathcal{C}(\cdot, \theta_l)$, $l = \{1, \dots, L\}$, the dimension of the output \mathbf{C}_L of the L^{th} layer $\mathcal{C}(\cdot, \theta_L)$ should be $Q_t \times I_t \times 2M$. However, the dimension of \mathbf{C}_L is determined by the architectural parameters of the CL in $\mathcal{C}(\cdot, \theta_l)$, $l = \{1, \dots, L\}$ such as the number of convolution kernel and the sizes of convolution kernel, sliding step, zero padding. Consequently, in what follows, we derive some architectural conditions for the CL in $\mathcal{C}(\cdot, \theta_l)$, $l = \{1, \dots, L\}$ to satisfy Remark 3.

Proposition 1: Let $w_{\mathcal{C}(\cdot, \theta_l)}^{\text{in}}$, $h_{\mathcal{C}(\cdot, \theta_l)}^{\text{in}}$, $w_{\mathcal{C}(\cdot, \theta_l)}^{\text{out}}$ and $h_{\mathcal{C}(\cdot, \theta_l)}^{\text{out}}$ denote the input-output width and height of $\mathcal{C}(\cdot, \theta_l)$, as well as k_l^w , k_l^h , p_l^w , p_l^h , s_l^w and s_l^h denote the width and height of the convolution kernel, the zero padding, the sliding step for the CL of $\mathcal{C}(\cdot, \theta_l)$, respectively. When $s_l^w = 1$, $s_l^h = 1$, if $p_l^w = \frac{1}{2}(k_l^w - 1)$, $p_l^h = \frac{1}{2}(k_l^h - 1)$, both p_l^w , p_l^h and k_l^w , k_l^h are positive integers, then $w_{\mathcal{C}(\cdot, \theta_l)}^{\text{out}} = w_{\mathcal{C}(\cdot, \theta_l)}^{\text{in}}$ and $h_{\mathcal{C}(\cdot, \theta_l)}^{\text{out}} = h_{\mathcal{C}(\cdot, \theta_l)}^{\text{in}}$.

Proof: As can be seen in Fig.1, $\mathcal{C}(\cdot, \theta_l)$ contains a CL, a BN and an AL. For the CL in $\mathcal{C}(\cdot, \theta_l)$, its output width and height $w_{\mathcal{C}(\cdot, \theta_l)}^{\text{CL}} \times h_{\mathcal{C}(\cdot, \theta_l)}^{\text{CL}}$ are denoted as

$$\begin{cases} w_{\mathcal{C}(\cdot, \theta_l)}^{\text{CL}} = \frac{w_{\mathcal{C}(\cdot, \theta_l)}^{\text{in}} + 2p_l^w - k_l^w}{s_l^w} + 1, \\ h_{\mathcal{C}(\cdot, \theta_l)}^{\text{CL}} = \frac{h_{\mathcal{C}(\cdot, \theta_l)}^{\text{in}} + 2p_l^h - k_l^h}{s_l^h} + 1, \end{cases} \quad (5)$$

where $s_l^w = 1$, $s_l^h = 1$, $p_l^w = \frac{1}{2}(k_l^w - 1)$ and $p_l^h = \frac{1}{2}(k_l^h - 1)$ are brought into Eq.(5),

$$\begin{cases} w_{\mathcal{C}(\cdot, \theta_l)}^{\text{CL}} = \frac{w_{\mathcal{C}(\cdot, \theta_l)}^{\text{in}} + 2 \times \frac{1}{2}(k_l^w - 1) - k_l^w}{1} + 1 = w_{\mathcal{C}(\cdot, \theta_l)}^{\text{in}}, \\ h_{\mathcal{C}(\cdot, \theta_l)}^{\text{CL}} = \frac{h_{\mathcal{C}(\cdot, \theta_l)}^{\text{in}} + 2 \times \frac{1}{2}(k_l^h - 1) - k_l^h}{1} + 1 = h_{\mathcal{C}(\cdot, \theta_l)}^{\text{in}}. \end{cases} \quad (6)$$

Based on Eq.(6), the output width and height of the CL in $\mathcal{C}(\cdot, \theta_l)$ are $w_{\mathcal{C}(\cdot, \theta_l)}^{\text{in}}$ and $h_{\mathcal{C}(\cdot, \theta_l)}^{\text{in}}$, respectively. On the other hand, the BN and AL do not change the input dimension, i.e., the output width and height of the BN and AL in $\mathcal{C}(\cdot, \theta_l)$ are also $w_{\mathcal{C}(\cdot, \theta_l)}^{\text{in}}$ and $h_{\mathcal{C}(\cdot, \theta_l)}^{\text{in}}$, respectively. Consequently, the output width and height of $\mathcal{C}(\cdot, \theta_l)$ are $w_{\mathcal{C}(\cdot, \theta_l)}^{\text{in}}$ and $h_{\mathcal{C}(\cdot, \theta_l)}^{\text{in}}$, i.e., $w_{\mathcal{C}(\cdot, \theta_l)}^{\text{out}} = w_{\mathcal{C}(\cdot, \theta_l)}^{\text{in}}$ and $h_{\mathcal{C}(\cdot, \theta_l)}^{\text{out}} = h_{\mathcal{C}(\cdot, \theta_l)}^{\text{in}}$, respectively. ■

Proposition 2: When $s_l^w > 1$, $s_l^h > 1$, if $p_l^w = \frac{1}{2}(w_{\mathcal{C}(\cdot, \theta_l)}^{\text{in}} s_l^w - w_{\mathcal{C}(\cdot, \theta_l)}^{\text{in}} - s_l^w + k_l^w)$ and $p_l^h = \frac{1}{2}(h_{\mathcal{C}(\cdot, \theta_l)}^{\text{in}} s_l^h - h_{\mathcal{C}(\cdot, \theta_l)}^{\text{in}} - s_l^h + k_l^h)$, as well as p_l^w , p_l^h , s_l^w , s_l^h , k_l^w , k_l^h are positive integers, then $w_{\mathcal{C}(\cdot, \theta_l)}^{\text{out}} = w_{\mathcal{C}(\cdot, \theta_l)}^{\text{in}}$ and $h_{\mathcal{C}(\cdot, \theta_l)}^{\text{out}} = h_{\mathcal{C}(\cdot, \theta_l)}^{\text{in}}$.

Proof: For the CL in $\mathcal{C}(\cdot, \theta_l)$, where $s_l^w > 1$, $s_l^h > 1$, $p_l^w = \frac{1}{2}(w_{\mathcal{C}(\cdot, \theta_l)}^{\text{in}} s_l^w - w_{\mathcal{C}(\cdot, \theta_l)}^{\text{in}} - s_l^w + k_l^w)$ and $p_l^h = \frac{1}{2}(h_{\mathcal{C}(\cdot, \theta_l)}^{\text{in}} s_l^h - h_{\mathcal{C}(\cdot, \theta_l)}^{\text{in}} - s_l^h + k_l^h)$, its output width and height $w_{\mathcal{C}(\cdot, \theta_l)}^{\text{CL}} \times h_{\mathcal{C}(\cdot, \theta_l)}^{\text{CL}}$

are denoted as

$$\begin{cases} w_{\mathcal{C}(\cdot, \theta_l)}^{\text{CL}} = \frac{w_{\mathcal{C}(\cdot, \theta_l)}^{\text{in}} + 2 \times \frac{1}{2}(w_{\mathcal{C}(\cdot, \theta_l)}^{\text{in}} s_l^w - w_{\mathcal{C}(\cdot, \theta_l)}^{\text{in}} - s_l^w + k_l^w) - k_l^w}{s_l^w} \\ \quad + 1 = w_{\mathcal{C}(\cdot, \theta_l)}^{\text{in}}, \\ h_{\mathcal{C}(\cdot, \theta_l)}^{\text{CL}} = \frac{h_{\mathcal{C}(\cdot, \theta_l)}^{\text{in}} + 2 \times \frac{1}{2}(h_{\mathcal{C}(\cdot, \theta_l)}^{\text{in}} s_l^h - h_{\mathcal{C}(\cdot, \theta_l)}^{\text{in}} - s_l^h + k_l^h) - k_l^h}{s_l^h} \\ \quad + 1 = h_{\mathcal{C}(\cdot, \theta_l)}^{\text{in}}. \end{cases} \quad (7)$$

Similarly, the output width and height of $\mathcal{C}(\cdot, \theta_l)$ are $w_{\mathcal{C}(\cdot, \theta_l)}^{\text{in}}$ and $h_{\mathcal{C}(\cdot, \theta_l)}^{\text{in}}$, i.e., $w_{\mathcal{C}(\cdot, \theta_l)}^{\text{out}} = w_{\mathcal{C}(\cdot, \theta_l)}^{\text{in}}$ and $h_{\mathcal{C}(\cdot, \theta_l)}^{\text{out}} = h_{\mathcal{C}(\cdot, \theta_l)}^{\text{in}}$. ■

Obviously, as long as the architectures k_l^w , k_l^h , p_l^w , p_l^h , s_l^w and s_l^h in each $\mathcal{C}(\cdot, \theta_l)$ satisfy Proposition 1 or Proposition 2, the width and height of \mathbf{C}_L are $Q_t \times I_t$. In addition, if the number of convolutional kernels c_L for the L^{th} layer $\mathcal{C}(\cdot, \theta_L)$ is set to $2M$, then the dimension of \mathbf{C}_L is $Q_t \times I_t \times 2M$. On the other hand, based on Proposition 1 or Proposition 2, when the dimension of the input 3D real-valued CSI $\mathbf{H}_{t,\text{mod}}^{\text{3D}}$ changes from $Q_t \times I_t \times MN$ to $Q_{t'} \times I_{t'} \times MN$ at the t' period, then the dimension of \mathbf{C}_L also varies from $Q_t \times I_t \times 2M$ to $Q_{t'} \times I_{t'} \times 2M$. Consequently, the architectural conditions that satisfy the constraint $(Q_t, I_t) \Leftarrow t, \forall t \in \mathcal{T}$ in the optimization problem (3) are summarized in Remark 4.

Remark 4: The constraint $(Q_t, I_t) \Leftarrow t, \forall t \in \mathcal{T}$ in the optimization problem (3) is satisfied, if only the following conditions are held as

- 1) The architectural parameters k_l^w , k_l^h , p_l^w , p_l^h , s_l^w , s_l^h , $l = 1, \dots, L$ in each $\mathcal{C}(\cdot, \theta_l)$ satisfy Proposition 1 or Proposition 2.
- 2) The number of convolutional kernels c_L for $\mathcal{C}(\cdot, \theta_L)$ is equal to $2M$.

In summary, based on Proposition 1, Proposition 2 and Remark 4, as long as the two conditions in Remark 4 are satisfied, $\mathcal{C}(\cdot, \theta_l)$ maps CSI to beamforming with satisfying $(Q_t, I_t) \Leftarrow t, \forall t \in \mathcal{T}$ in the optimization problem (3).

C. High-Generalization Beamforming Module $\mathcal{G}(\cdot, \theta_l)$

$\mathcal{C}(\cdot, \theta_l)$ has been solved for dynamic wireless environments with the varying numbers of APs and users $(Q_t, I_t) \Leftarrow t, \forall t \in \mathcal{T}$ in cell-free systems as long as the two conditions in Remark 4 are satisfied. In the following, under the conditions specified in Remark 4, $\mathcal{G}(\cdot, \theta_l)$ is designed to improve the generalization performance of $D(\mathbf{H}_t) \Leftarrow t, \forall t \in \mathcal{T}$ in the optimization problem (3), by processing the output \mathbf{C}_l of $\mathcal{C}(\cdot, \theta_l)$ to obtain the valuable features of the varying channels. Especially, $\mathcal{G}(\cdot, \theta_l)$ includes a distinguishing sensitive feature module and a discarding sensitive feature module.

1) **Distinguishing Sensitive Feature Module:** $\mathcal{C}(\cdot, \theta_l)$ aims at the real-time beamforming design, whereas the purpose of $\mathcal{G}(\cdot, \theta_l)$ is to obtain the valuable features of the varying channels. These are two different tasks. To address this, a commonly used simple gradient reversal layer (GRL) [25] is added between these two tasks. The GRL transforms the gradient into a negative gradient in the gradient backpropagation, which forms an adversarial training to find a balance between the above two tasks, and please refer to [25] for more details.

On the other hand, the output $\mathbf{C}_l \in \mathbb{R}^{Q_t \times I_t \times C}$ of $\mathcal{C}(\cdot, \theta_l)$ contains C features with dimension $Q_t \times I_t$. To determine which features contain sensitive information for the varying channels, this work designs a sensitive feature discriminator $\mathcal{D}(\cdot, \theta_l)$ containing a global average pooling (GAP) layer and a fully connected (FC) layer. Specifically, $\mathcal{D}(\cdot, \theta_l)$ first utilizes GAP to process $\mathbf{C}_l \in \mathbb{R}^{Q_t \times I_t \times C}$ to obtain global features \mathbf{g}_l for reducing computational complexity, which is denoted as

$$\mathbf{g}_l = \text{GAP}(\mathbf{C}_l) \in \mathbb{R}^C. \quad (8)$$

Afterwards, \mathbf{g}_l is fed into the FC layer, where the number of the input-output neurons of the FC layer is C and T , respectively. Meanwhile, a sensitive feature discriminator loss function $\mathcal{L}_l^{\text{dis}}$ is minimized to train $\mathcal{D}(\cdot, \theta_l)$, i.e.,

$$\mathcal{L}_l^{\text{dis}} = -\frac{1}{T} \sum_{t=1}^T \sum_{t'=1}^T \mathbb{1}_{[t=t']} \log \mathcal{D}(\mathbf{g}_l, \theta_l), \quad (9)$$

where $\mathbb{1}_{[t=t']}$ denotes an indicator function, i.e., if the index t is equal to t' , then $\mathbb{1}_{[t=t']} = 1$, otherwise $\mathbb{1}_{[t=t']} = 0$.

Note that an intuitive finding can be obtained for $\mathcal{D}(\cdot, \theta_l)$. That is, the features contributing most to the prediction of $\mathcal{D}(\cdot, \theta_l)$ may contain sensitive features to the varying channels, since the inputs and outputs of $\mathcal{D}(\cdot, \theta_l)$ are the features and the number of the varying channels, respectively. Consequently, this paper defines a score \mathbf{s}_l to represent the contribution of the features, computed as the dot product of $\mathbf{g}_l \in \mathbb{R}^C$ and the weighted activations $\mathbf{w}_l^{\text{cor}} \in \mathbb{R}^C$ of the FC layer for the correct prediction of $\mathcal{D}(\cdot, \theta_l)$, as the weighted activations indicate the importance of the input data [26]. Formally, it can be denoted as

$$\mathbf{s}_l = \mathbf{w}_l^{\text{cor}} \otimes \mathbf{g}_l \in \mathbb{R}^C, \quad (10)$$

where \otimes denotes the dot product. Obviously, when the value of the element in $\mathbf{s}_l \in \mathbb{R}^C$ is larger, its corresponding feature is more sensitive to the varying channels, and vice versa.

2) *Discarding Sensitive Feature Module*: Based on $\mathbf{s}_l \in \mathbb{R}^C$, this work explicitly discards some sensitive features to the varying channels during the training stage. Specifically, given $\mathbf{s}_l \in \mathbb{R}^C$, this work computes the probability p_l^c of discarding the c^{th} feature of dimension $Q_t \times I_t$ in $\mathbf{C}_l \in \mathbb{R}^{Q_t \times I_t \times C}$, i.e.,

$$p_l^c = \frac{s_l^c}{\sum_{c=1}^C s_l^c}, \quad (11)$$

where s_l^c denotes the c^{th} element in $\mathbf{s}_l = [s_l^1, \dots, s_l^c, \dots, s_l^C] \in \mathbb{R}^C$.

Subsequently, based on $\mathbf{p}_l = [p_l^1, \dots, p_l^c, \dots, p_l^C] \in \mathbb{R}^C$, a weighted random selection (WRS) algorithm [27] is applied to generate the binary mask, since it is highly computationally efficient with complexity $O(C)$. To be more concrete, for the c^{th} feature of dimension $Q_t \times I_t$ in $\mathbf{C}_l \in \mathbb{R}^{Q_t \times I_t \times C}$ with probability p_l^c , a random number $r_l^c \in (0, 1)$ is generated, where a key value k_l^c is computed as

$$k_l^c = r_l^c \frac{1}{p_l^c}. \quad (12)$$

³Note that *Remark 4* only requires the third dimension of \mathbf{C}_L to be $2M$, and has no requirement for the other $\mathbf{C}_l, l = \{1, \dots, L-1\}$. For simplicity, let \mathbf{C} be collectively referred to the third dimension of \mathbf{C}_l , i.e., $\mathbf{C}_l \in \mathbb{R}^{Q_t \times I_t \times C}$.

When s_l^c is larger, both p_l^c and k_l^c increase, indicating that the feature of dimension $Q_t \times I_t$ in $\mathbf{C}_l \in \mathbb{R}^{Q_t \times I_t \times C}$ is more sensitive, and vice versa. Consequently, to discard the sensitive features and retain the valuable features for the varying channels, the C_{dis} items with the largest key values are selected, and their corresponding mask values are set to 0, i.e.,

$$m_l^c = \begin{cases} 0 & \text{if } c \in \text{TOP}([k_l^1, \dots, k_l^c, \dots, k_l^C], C_{\text{dis}}), \\ 1 & \text{otherwise,} \end{cases} \quad (13)$$

where $c \in \text{TOP}([k_l^1, \dots, k_l^c, \dots, k_l^C], C_{\text{dis}})$ denotes the C_{dis} items with the largest key.

Afterwards, the binary mask $\mathbf{m}_l = [m_l^1, \dots, m_l^c, \dots, m_l^C] \in \mathbb{R}^C$ is dot-multiplied with \mathbf{C}_l to obtain the valuable features \mathbf{G}_l for the varying channels, which is defined as

$$\mathbf{G}_l = \mathbf{m}_l \otimes \mathbf{C}_l \in \mathbb{R}^{Q_t \times I_t \times C}. \quad (14)$$

It is obvious that \mathbf{G}_l effectively extracts the valuable features for the varying channels via the binary mask to discard the sensitive features. Remarkably, $\mathcal{G}(\cdot, \theta_l)$ is only added after $\mathbf{C}_l, l = \{1, \dots, L-1\}$ without \mathbf{C}_L to guarantee that the output beamforming of HGNet is a real-valued tensor of dimension $Q_t \times I_t \times 2M$ with $\mathbf{H}_{t,\text{mod}}^{3\text{D}} \in \mathbb{R}^{Q_t \times I_t \times MN}$ as the input.

D. Output

Before the output beamforming, an identity mapping is added to construct the residual structure for effectively avoiding the gradient vanishing problem [28], which is denoted as

$$\mathbf{V}_{t,\text{rea}}^{3\text{D}} = \text{AL}(\mathbf{C}_L + \mathbf{V}_{\text{IM}}) \in \mathbb{R}^{Q_t \times I_t \times 2M}, \quad (15)$$

where \mathbf{V}_{IM} denotes the output of the identity mapping with $\mathbf{H}_{t,\text{mod}}^{3\text{D}} \in \mathbb{R}^{Q_t \times I_t \times MN}$ as the input. Afterwards, the output module first transforms $\mathbf{V}_{t,\text{rea}}^{3\text{D}} \in \mathbb{R}^{Q_t \times I_t \times 2M}$ into a 3D complex-valued beamforming tensor $\mathbf{V}_{t,\text{com}}^{3\text{D}} \in \mathbb{C}^{Q_t \times I_t \times M}$ as follows

$$\mathbf{V}_{t,\text{com}}^{3\text{D}} = \mathbf{V}_{t,\text{rea}}^{3\text{D}}[:, :, 0 : M] + j\mathbf{V}_{t,\text{rea}}^{3\text{D}}[:, :, M : 2M]. \quad (16)$$

On the other hand, $\mathbf{V}_{t,\text{com}}^{3\text{D}}$ also needs to satisfy the power constraint. Since this is a convex constraint [29], it can be satisfied using a projection function. Consequently, following [29], the output module applies the following projection function to satisfy the power constraint, i.e.,

$$\mathbf{v}_{i,t}^q = \begin{cases} \mathbf{v}_{i,t}^q & \text{if } \sum_{i=1}^{I_t} \mathbf{v}_{i,t}^{q,H} \mathbf{v}_{i,t}^q \leq P_{\max}, \\ \frac{\mathbf{v}_{i,t}^q}{\sum_{i=1}^{I_t} \mathbf{v}_{i,t}^{q,H} \mathbf{v}_{i,t}^q} P_{\max} & \text{otherwise.} \end{cases} \quad (17)$$

Finally, following the commonly utilized unsupervised training method [30], we also take the negative of the sum SE as the loss function to train HGNet, where the output beamforming of HGNet is denoted as $\mathbf{V}_{t,\text{HGNet}}^{3\text{D}} \in \mathbb{C}^{Q_t \times I_t \times M}$.

E. Theoretical Analysis of High-Generalization of HGNet

In this subsection, the bias of the varying channels is measured by the commonly known maximum mean discrepancy (MMD) distance. It is a metric that quantifies the difference between the data distribution in the source and the target domains [31]. It is defined as follows.

Definition 1: (MMD [32]) Let $\mathcal{F} = \{f \in \mathcal{H}_k : \|f\|_{\mathcal{H}_k} \leq 1\}$ denote the set of functions on the sample space, in which \mathcal{H}_k is a reproducing kernel Hilbert space (RKHS) with kernel function k . Let \mathcal{S}_{tr} and \mathcal{T}_{in} denote the source domain of the training stage and the target domain of the inference stage, where $\hat{\mathcal{S}}_{tr}$ and $\hat{\mathcal{T}}_{in}$ denote the D data sampled from \mathcal{S}_{tr} and \mathcal{T}_{in} , respectively. The MMD distance between $\hat{\mathcal{S}}_{tr}$ and $\hat{\mathcal{T}}_{in}$ is defined as

$$d_{MMD}(\hat{\mathcal{S}}_{tr}, \hat{\mathcal{T}}_{in}) = \sup_{f \in \mathcal{F}} \left[\frac{1}{D} \sum_{d=1}^D f(x_d) - \frac{1}{D} \sum_{d=1}^D f(y_d) \right],$$

where x_d and y_d denote the d^{th} data in $\hat{\mathcal{S}}_{tr}$ and $\hat{\mathcal{T}}_{in}$, respectively.

To facilitate analysis for the high generalization of $\mathcal{G}(\cdot, \theta_l)$ in HGNet, similar to MMD in Definition 1, a G-MMD is defined as follows.

Definition 2: (G-MMD) Following the definition in MMD, G-MMD distance between $\hat{\mathcal{S}}_{tr}$ and $\hat{\mathcal{T}}_{in}$ is defined as

$$d_{G-MMD}(\hat{\mathcal{S}}_{tr}, \hat{\mathcal{T}}_{in}) = \frac{1}{C} \sum_{c=1}^C \sup_{f_c \in \mathcal{F}_c} \left[\frac{1}{D} \sum_{d=1}^D f_c(\mathbf{G}_l[:, :, c])_{\hat{\mathcal{S}}_{tr}}^d - \frac{1}{D} \sum_{d=1}^D f_c(\mathbf{G}_l[:, :, c])_{\hat{\mathcal{T}}_{in}}^d \right],$$

where $(\mathbf{G}_l[:, :, c])_{\hat{\mathcal{S}}_{tr}}^d$ and $(\mathbf{G}_l[:, :, c])_{\hat{\mathcal{T}}_{in}}^d$ denote the c^{th} features of dimension $Q_t \times I_t$ in the output of $\mathcal{G}(\cdot, \theta_l)$ when the d^{th} data in $\hat{\mathcal{S}}_{tr}$ and $\hat{\mathcal{T}}_{in}$ are inputted to HGNet, respectively. $\mathcal{F}_c = \{f_c \in \mathcal{H}_k : \|f_c\|_{\mathcal{H}_k} \leq 1\}$ denotes the set of functions on the sample space corresponding to $\mathbf{G}_l[:, :, c]$.

Proposition 3: With the previous definitions, let $\mathcal{S}_{tr}^t, t \in \mathcal{T}$ denote the source domain of the training stage for T varying channels, where $\hat{\mathcal{S}}_{tr}^t$ denote the D data sampled from \mathcal{S}_{tr}^t . Let $R_{\mathcal{T}_{in}}[\mathcal{G}]$ denote the generalized risk bound of $\mathcal{G}(\cdot, \theta_l)$ in HGNet for the target domain \mathcal{T}_{in} . With the probability of at least $1 - \delta, \delta \in (0, 1)$, the following inequality holds for $R_{\mathcal{T}_{in}}[\mathcal{G}]$:

$$R_{\mathcal{T}_{in}}[\mathcal{G}] \leq \sup_{t, t' \in \mathcal{T}} d_{G-MMD}(\mathcal{S}_{tr}^{t'}, \mathcal{S}_{tr}^t) + d_{G-MMD}(\hat{\mathcal{T}}_{in}, \bar{\mathcal{T}}_{in}) + \varpi + \varrho + \xi,$$

where $\bar{\mathcal{T}}_{in} = \sum_{t=1}^T \kappa_t \mathcal{S}_{tr}^t$ denotes a mixture of T varying channels closest to the target domain \mathcal{T}_{in} , and the mixture weight is given by $\sum_{t=1}^T \kappa_t = 1$. $\hat{\mathcal{T}}_{in}$ denotes the D data sampled from $\bar{\mathcal{T}}_{in}$. $\varpi = \sum_{t=1}^T \kappa_t R_{\mathcal{S}_{tr}^t}[\mathcal{G}]$ denotes the mixture weight of the generalization error for known source domains $\mathcal{S}_{tr}^t, t \in \mathcal{T}$. $\varrho = R_{\mathcal{T}_{in}}[\mathcal{G}^*] + R_{\mathcal{T}_{in}}[\mathcal{G}^*]$ denotes the combined error of ideal $\mathcal{G}^*(\cdot, \theta_l^*)$. $\xi = \frac{2}{D} \left(\sum_{t=1}^T \kappa_t \mathbb{E} \left[\sqrt{\text{tr}(k_{\hat{\mathcal{S}}_{tr}^t})} \right] + \mathbb{E} \left[\sqrt{\text{tr}(k_{\hat{\mathcal{T}}_{in}})} \right] \right) + 2\sqrt{\frac{\log(\frac{2}{\delta})}{2D}}$, in which $k_{\hat{\mathcal{S}}_{tr}^t}$ and $k_{\hat{\mathcal{T}}_{in}}$ denote kernel functions computed on samples from $\hat{\mathcal{S}}_{tr}^t$ and $\hat{\mathcal{T}}_{in}$, respectively.

Proof: Please see Appendix A for the detailed proof. ■

From Proposition 3, it is clear that $\sup_{t, t' \in \mathcal{T}} d_{G-MMD}(\mathcal{S}_{tr}^{t'}, \mathcal{S}_{tr}^t)$

and $d_{G-MMD}(\hat{\mathcal{T}}_{in}, \bar{\mathcal{T}}_{in})$ mainly determine the upper bound of the generalization error of $\mathcal{G}(\cdot, \theta_l)$ in HGNet. To be concrete, $\sup_{t, t' \in \mathcal{T}} d_{G-MMD}(\mathcal{S}_{tr}^{t'}, \mathcal{S}_{tr}^t)$ denotes the G-MMD distance of the output \mathbf{G}_l of $\mathcal{G}(\cdot, \theta_l)$ for any pair of the varying channels in the source domain of the training stage. Since the output \mathbf{G}_l of $\mathcal{G}(\cdot, \theta_l)$ explicitly discards the sensitive features to the varying channels during the training stage, this can promote $\mathcal{G}(\cdot, \theta_l)$ to learn a model that extracts non-sensitive features for the varying channels, i.e., effectively reducing $\sup_{t, t' \in \mathcal{T}} d_{G-MMD}(\mathcal{S}_{tr}^{t'}, \mathcal{S}_{tr}^t)$. On the other hand, $d_{G-MMD}(\hat{\mathcal{T}}_{in}, \bar{\mathcal{T}}_{in})$ denotes the G-MMD distance of the output \mathbf{G}_l of $\mathcal{G}(\cdot, \theta_l)$ for source domain $\mathcal{S}_{tr}^t, t \in \mathcal{T}$ and target domain \mathcal{T}_{in} . After removing the sensitive features to the varying channels, the features extracted from the target domain \mathcal{T}_{in} would become more similar to those of the source domains $\mathcal{S}_{tr}^t, t \in \mathcal{T}$, thus also decreasing $d_{G-MMD}(\hat{\mathcal{T}}_{in}, \bar{\mathcal{T}}_{in})$. In summary, based on Proposition 3, $\mathcal{G}(\cdot, \theta_l)$ obtains a lower upper bound of the generalization error, which guarantees that HGNet yields a better sum SE performance for $D(\mathbf{H}_t) \leftarrow t, \forall t \in \mathcal{T}$ in the optimization problem (3).

IV. OAU ALGORITHM

To realize the online adaptive real-time beamforming design to further improve the sum SE performance of dynamic wireless environments with the varying channels and the different numbers of APs and users in cell-free systems, the OAU algorithm is proposed in this section. Intuitively, it is a natural choice to adaptively update the parameters of HGNet online by taking the negative of the sum SE as a loss function. Despite the simplicity of this approach, it suffers from two major problems.

- 1) The parameters of HGNet are normally high-dimensional, and updating the entire parameters is time-consuming without fulfilling the requirements of the real-time beamforming design.
- 2) Since computing the sum SE involves the matrix inversion with high computational complexity, it is also difficult to satisfy the real-time beamforming design when updating the parameters of HGNet with the negative sum SE as the loss function.

To solve the first problem, the proposed OAU algorithm online adaptively updates the affine parameters of the BN layer in HGNet instead of the entire parameters of HGNet. This is because the affine parameters comprise less than 3% of the total number of parameters in HGNet. Consequently, updating the affine parameters of the BN layer is more computationally efficient, and suitable for the real-time beamforming design. Concretely, to simplify notation, the input of the BN layer at the l^{th} layer $\mathcal{C}(\cdot, \theta_l)$ of HGNet is defined as $\mathbf{X}_l = \text{CL}(\mathbf{G}_{l-1}, \theta_l) \in \mathbb{R}^{Q_t \times I_t \times C}$. The BN layer first calculates the normalized value of $\mathbf{X}_l \in \mathbb{R}^{Q_t \times I_t \times C}$ as

$$\mathbf{X}_l^{\text{nor}} = \frac{\mathbf{X}_l - \mathbb{E}[\mathbf{X}_l]}{\sqrt{\text{Var}[\mathbf{X}_l] + \epsilon}}, \quad (18)$$

where ϵ denotes a very small constant to avoid a zero in the denominator. $E[\mathbf{X}_l]$ and $\text{Var}[\mathbf{X}_l]$ denote the mean and variance of \mathbf{X}_l , respectively. Since the input CSI in the inference stage is a single input rather than a mini-batch as in the training phase, it is more challenging to compute $E[\mathbf{X}_l]$ and $\text{Var}[\mathbf{X}_l]$. As a result, following the widely applied approach of deep learning, the unbiased estimation for the mean and variance of the mini-batch of the training phase over the total training dataset is used as $E[\mathbf{X}_l]$ and $\text{Var}[\mathbf{X}_l]$, which are denoted as

$$E[\mathbf{X}_l] \leftarrow \mathbb{E}_D[\mu_l], \text{Var}[\mathbf{X}_l] \leftarrow \frac{B}{B-1} \mathbb{E}_D[\sigma_l^2], \quad (19)$$

where B denotes the mini-batch size of the training stage. $\mathbb{E}_D[\cdot]$ denotes the expectation over the total training dataset. μ_l and σ_l^2 denote the mean and variance on the mini-batch B for the input data of the BN layer at the l^{th} layer $\mathcal{C}(\cdot, \theta_l)$ of HGNet, respectively.

Subsequently, $\mathbf{X}_l^{\text{nor}}$ is transformed by the affine parameters to obtain the output of the BN layer at the l^{th} layer $\mathcal{C}(\cdot, \theta_l)$ of HGNet, which is denoted as

$$\mathbf{X}_l^{\text{bn}}[:, :, c] = \gamma_l^c \otimes \mathbf{X}_l^{\text{nor}}[:, :, c] + \beta_l^c, \quad (20)$$

where $\gamma_l = [\gamma_l^1, \dots, \gamma_l^c, \dots, \gamma_l^C] \in \mathbb{R}^C$ and $\beta_l = [\beta_l^1, \dots, \beta_l^c, \dots, \beta_l^C] \in \mathbb{R}^C$ denote the affine parameters of the scale and the shift of the BN layer at the l^{th} layer $\mathcal{C}(\cdot, \theta_l)$ of HGNet, which are learnable parameters. From Eqs.(18) to (20), \mathbf{X}_l^{bn} is determined by \mathbf{X}_l , $E[\mathbf{X}_l]$, $\text{Var}[\mathbf{X}_l]$, ϵ , γ_l , β_l , where $E[\mathbf{X}_l]$, $\text{Var}[\mathbf{X}_l]$ and ϵ are constants after training. Therefore, \mathbf{X}_l^{bn} can be changed to improve the sum SE performance of the beamforming design by online adaptively updating γ_l and β_l in the inference phase.

On the other hand, updating γ_l and β_l also requires an objective function. This can be selected to the negative value of the sum SE as a loss function to update γ_l and β_l via the gradient descent algorithm. Unfortunately, the computation of sum SE typically involves high-dimensional matrix inverse operations, which hinders the realization of the online adaptive real-time beamforming design. As a remedy, this work uses information entropy as an objective function to optimize γ_l and β_l . This is because the information entropy is highly computationally efficient, relying only on simple dot product and summation operations without matrix inversion. In addition, the information entropy can measure error and bias, which ensures to learn a better model [33]. Formally, this is denoted as

$$\mathcal{L}_{\text{ie}} = - \sum_{q=1}^{Q_t} \sum_{i=1}^{I_t} \sum_{c=1}^M |\mathbf{V}_{t, \text{HGNet}}^{\text{3D}}[q, i, c] \otimes \log \mathbf{V}_{t, \text{HGNet}}^{\text{3D}}[q, i, c]|. \quad (21)$$

In summary, by minimizing \mathcal{L}_{ie} to adaptively update γ_l and β_l online, the proposed OAU algorithm effectively solves the above two problems. This also enables the online adaptive real-time beamforming design for dynamic wireless environments with the varying channels and the different numbers of APs and users. The pseudocode of the proposed OAU algorithm is summarized in Algorithm 1.

Algorithm 1: Proposed OAU Algorithm

Input: Trained HGNet, number of layers of HGNet L , \mathbf{H}_t , number of updates H , learning rate R ;
Output: $\mathbf{V}_{t, \text{HGNet}}^{\text{3D}}$;
Initialize $(E[\mathbf{X}_l], \text{Var}[\mathbf{X}_l], \epsilon, \gamma_l, \beta_l) \leftarrow$ Trained HGNet;
for $h \leftarrow 1 : H$ **do**
 for $l \leftarrow 1 : L$ **do**
 $\mathbf{X}_l^{\text{nor}} \leftarrow$ Calculate the BN normalization of \mathbf{H}_t at the l^{th} layer $\mathcal{C}(\cdot, \theta_l)$ of HGNet by Eq.(18);
 $\mathbf{X}_l^{\text{bn}} \leftarrow$ Calculate the BN output of \mathbf{H}_t at the l^{th} layer $\mathcal{C}(\cdot, \theta_l)$ of HGNet by Eq.(20);
 end
 $\mathcal{L}_{\text{ie}} \leftarrow$ Calculate the loss function by Eq.(21);
 while $l > 0$ **do**
 $\gamma_l \leftarrow \gamma_l - R \times \partial \mathcal{L}_{\text{ie}} / \partial \gamma_l$;
 $\beta_l \leftarrow \beta_l - R \times \partial \mathcal{L}_{\text{ie}} / \partial \beta_l$;
 $l \leftarrow l - 1$;
 end
end
 $\mathbf{V}_{t, \text{HGNet}}^{\text{3D}} \leftarrow$ Output beamforming by feeding \mathbf{H}_t into HGNet that have been online adaptively updated;
Return: $\mathbf{V}_{t, \text{HGNet}}^{\text{3D}}$;

V. EXPERIMENTAL RESULTS

In this section, we validate the effectiveness of the proposed HGNet with OAU algorithm. Specifically, we first introduce the experimental environments and system parameters. Then, we evaluate the performance of the proposed HGNet, followed by an assessment of the proposed OAU algorithm's performance. As benchmarks, the following schemes are compared:

- **WMMSE:** WMMSE [8] is a traditional optimization algorithm for the beamforming design. Its experimental results after 100 iterations serve as a benchmark, as a higher number of iterations brings the solution closer to optimality.
- **Limited WMMSE (L-WMMSE):** The number of iterations is set to match the number of layers in HGNet, and alignment comparisons are performed to verify the improved performance and computational efficiency of HGNet.
- **Edge-GNN:** Based on GNNs, [11] proposes Edge-GNN for cooperative beamforming design with better generalization performance.
- **SUNet:** Based on CNNs, [12] proposes SUNet with high computational efficiency to realize the beamforming design of cell-free systems.
- **HGNet w/o $\mathcal{G}(\cdot, \theta_l)$:** This variant excludes the high-generalization beamforming module $\mathcal{G}(\cdot, \theta_l)$ to specifically assess the contribution of this module to overall performance.

A. Experimental Setup

To characterize the varying channels of dynamic wireless environments, four commonly used channel models have been selected as follows.

• Channel 1: We utilize the geometric multi-path channel model [34], and the channel $\mathbf{H}_{i,t}^q \in \mathbb{C}^{M \times N}$ of the q^{th} AP to the i^{th} user at the t^{th} period can be expressed as

$$\mathbf{H}_{i,t}^q = \beta_{i,t}^q \sum_{p=1}^P \frac{g_{i,t,p}^q}{\sqrt{P}} \mathbf{a}_r(\phi_{i,t,p}^q) \mathbf{a}_t^H(\varphi_{i,t,p}^q), \quad (22)$$

where $\beta_{i,t}^q$ denotes the large-scale fading coefficient of the q^{th} AP to the i^{th} user at the t^{th} period. P denotes the number of propagation paths. $g_{i,t,p}^q \sim \mathcal{CN}(0, 1)$, $\varphi_{i,t,p}^q$ and $\phi_{i,t,p}^q$ denote the complex path gain, angles of departure and arrival, respectively. Moreover, \mathbf{a}_t and \mathbf{a}_r denote the array responses of transmitter.

For the other two channels, we adopt the channel model in [35] as follows

$$\mathbf{H}_{i,t}^q = \beta_{i,t}^q \left(\sqrt{\frac{\epsilon}{\epsilon+1}} \mathbf{a}_t(\varphi_{i,t}^q) \mathbf{a}_r^H(\phi_{i,t}^q) + \sqrt{\frac{1}{\epsilon+1}} \bar{\mathbf{H}}_{i,t}^q \right), \quad (23)$$

where $\varphi_{i,t}^q$ and $\phi_{i,t}^q$ denote the LoS directions of transmit and receive, respectively. $\bar{\mathbf{H}}_{i,t}^q$ denotes the NLoS component following the complex Gaussian distribution $\mathcal{CN}(\mathbf{0}, \mathbf{I})$.

- Channel 2: Rayleigh channel with $\epsilon = 0$.
- Channel 3: Rice channel with $\epsilon = 3$ dB.
- Channel 4: We also apply the ray-tracing channel in [36] to comprehensively validate the performance of the proposed method. Specifically, the shooting-and-bouncing rays (SBR) method is used as the simulation scheme for the ray-tracing channel model. Environmental data is then imported, and the scenario is accurately modeled using mathematical modeling tools. Next, all possible ray paths between transmitters and receivers are computed based on the geometrical optics and the uniform theory of diffraction. Finally, channel parameters such as path loss and angular spread are determined using the electromagnetic theory. For more details, please refer to Sect. III of [36].

Since different users may experience varying coherence times, the practical experiments, according to [37] and [38], set the coherence time to be the minimum of the coherence times experienced by all users to ensure that the system works reliably across networks. Formally, this can be expressed as

$$\tau_{\min} = \min \{ \tau_i \}, \quad (24)$$

where τ_i denotes the coherence time of the i^{th} user.

The proposed HGNet with OAU algorithm is implemented by PyTorch. For HGNet, the Adam optimizer is selected during the training stage. The learning rate and batch size are set to 64 and 0.1, respectively. The number of layers L for HGNet is set to 5, where the architectural parameters of each convolution unit $\mathcal{C}(\cdot, \theta_l)$ are set to $k_l^w = 3$, $k_l^h = 3$, $p_l^w = 1$, $p_l^h = 1$, $s_l^w = 1$, $s_l^h = 1$, $c_l = 2M$ to satisfy Propositions 1 or 2. Since the proposed HGNet operates under an unsupervised learning paradigm, this requires only CSI data without beamforming data during the training stage. For training CSI data, each channel model generates 6400 training samples by randomly scattering $Q = 16$ APs with $M = 4$ antennas and $I = 16$ users with $N = 2$ antennas within a $500 \times 500(m^2)$ coverage area. For better training, a total of 25600 data for the four channel

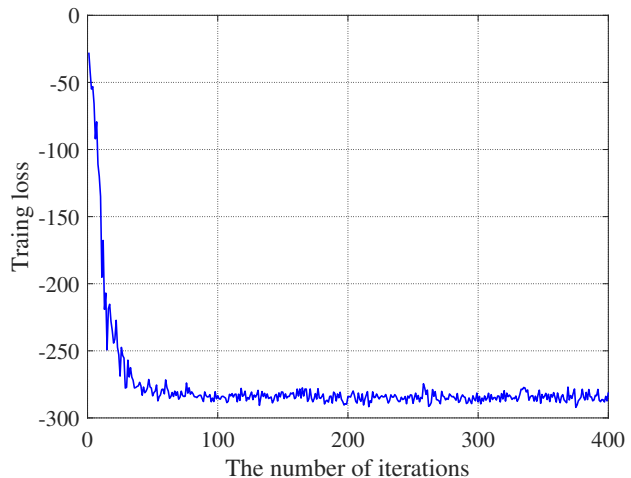


Fig. 3: Training loss graph.

TABLE I: Average computation time of the comparison algorithms for different numbers of APs and users.

Algorithms	$Q_t = 20, I_t = 20$	$Q_t = 20, I_t = 24$
WMMSE	61736.29ms	70391.51ms
L-WMMSE	1036.76ms	1292.65ms
Edge-GNN	7.78ms	9.37ms
SUNet	0.65ms	0.79ms
HGNet w/o $\mathcal{G}(\cdot, \theta_l)$	0.58ms	0.71ms
HGNet	0.47ms	0.57ms

models are randomly scrambled by utilizing the DataLoader database in Python. In addition, the training loss graph is shown in Fig.3. For OAU algorithm, the optimizer is also selected the Adam, where the learning rate R is set to 0.001.

B. Experimental Results for HGNet

To verify the effectiveness of the proposed HGNet on the varying channels and different numbers of APs and users, the average SE and computation time of these compared algorithms are shown in Figs.4-5 and Table I, respectively. Specifically, Fig.4 shows all users of each test sample exposed to the same channel model, where each channel model contains 640 test samples. In contrast, Fig.5 presents all users of each test sample under different channel models, in which each channel model randomly selects a quarter of all users. Due to the fact that all users in each test sample contain four channel models simultaneously, Fig.5 directly shows the average results of the different comparison algorithms over the 640 test samples. Since the average computation time is the same for all users exposed to the same and different channel models under the same number of APs and users condition, Table I only shows the average computation time for different numbers of APs and users for simplification. For Edge-GNN, SUNet, HGNet and HGNet w/o $\mathcal{G}(\cdot, \theta_l)$, the number of APs and users is fixed at $Q_t = 16, I_t = 16$ in the training stage. These trained deep learning methods during the inference stage

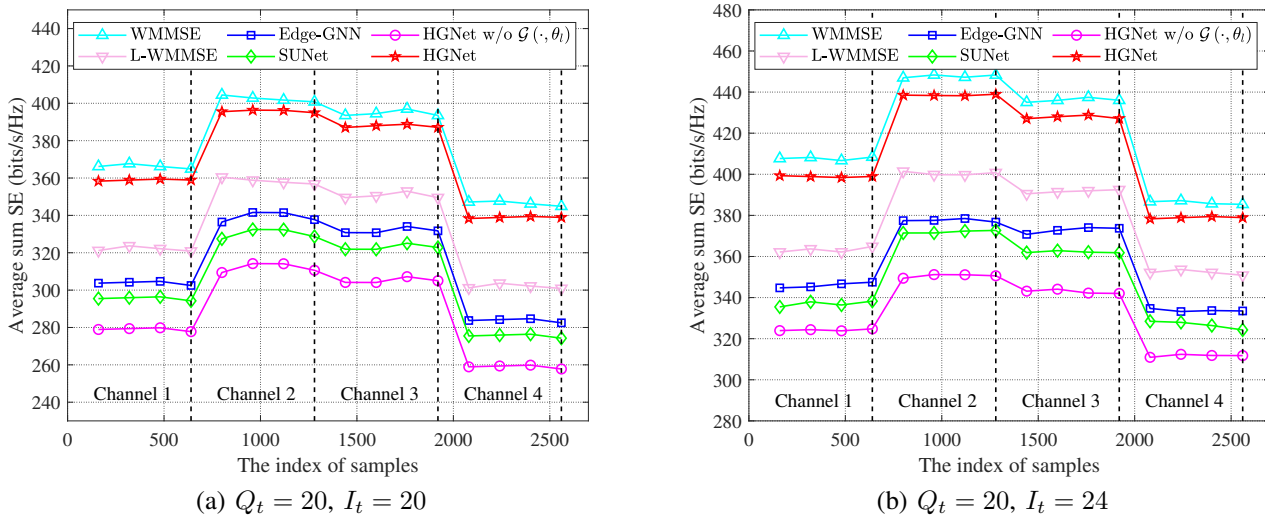


Fig. 4: Comparative results of average sum SE for all users of each test sample under the same channel model.

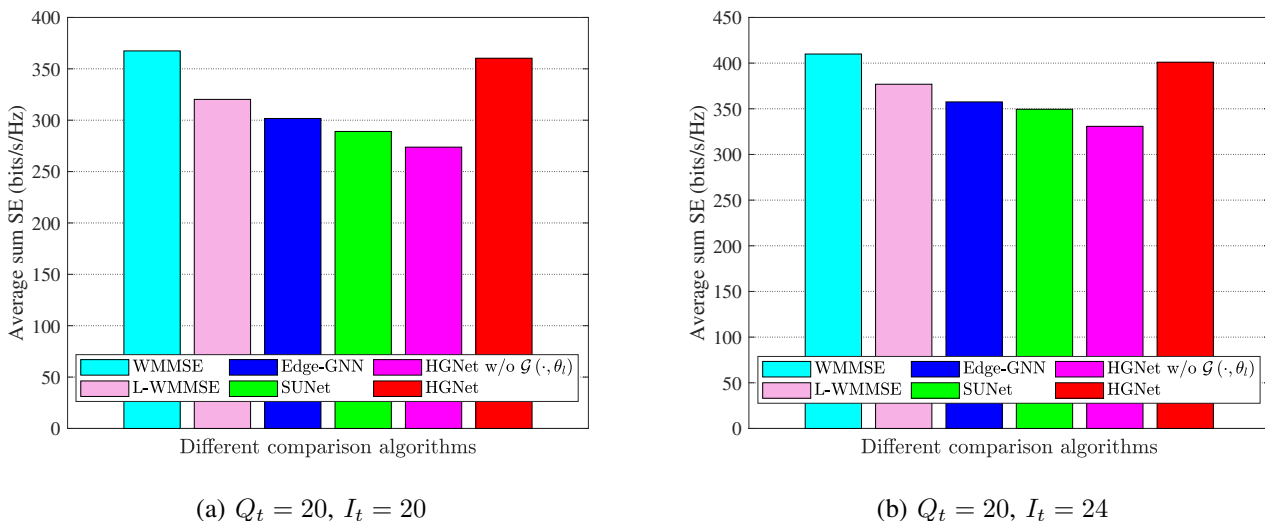


Fig. 5: Comparative results of average sum SE for all users of each test sample under different channel models.

are then generalized to the $Q_t = 20, I_t = 20$ scenario, where the number of APs is equal to the number of users, and to the $Q_t = 20, I_t = 24$ scenario, where the number of APs is unequal to the number of users, respectively. As WMMSE and L-WMMSE are traditional optimization algorithms without similar deep learning training and inference stages, it is applied directly in the $Q_t = 20, I_t = 20$ and $Q_t = 20, I_t = 24$ scenarios. By comparing the average SE of HGNet and HGNet w/o $\mathcal{G}(\cdot, \theta_l)$ in Figs.4-5, we observe that the high-generalization beamforming module $\mathcal{G}(\cdot, \theta_l)$ effectively improves the sum SE of the varying channels. This is because the high-generalization beamforming module $\mathcal{G}(\cdot, \theta_l)$ effectively extracts the valuable features for the varying channels. In addition, as can be seen from Table I, the average computation time of HGNet is also lower than that of HGNet w/o $\mathcal{G}(\cdot, \theta_l)$, since the high-generalization beamforming module $\mathcal{G}(\cdot, \theta_l)$

discards some sensitive features for the varying channels, thereby reducing computational complexity.

It can be seen from Figs.4-5 that the sum SE of HGNet is higher than those of L-WMMSE, SUNet and Edge-GNN, approaching that of WMMSE. The reasons are as follows. WMMSE with sufficient iterations provides the best sum SE performance, because it yields a stable solution for the beamforming design. However, as can be seen from Table I, its average computation time is 61736.29ms and 70391.51ms in the $Q_t = 20, I_t = 20$ and $Q_t = 20, I_t = 24$ scenarios, which is difficult to satisfy the real-time beamforming design. Reducing WMMSE's iterations to match HGNet's layers, the average computation time of L-WMMSE is 1036.76ms and 1292.65ms for the same scenarios, but it is still about 2000 times higher than HGNet. Moreover, the average sum SE of L-WMMSE is also lower than that of HGNet due to

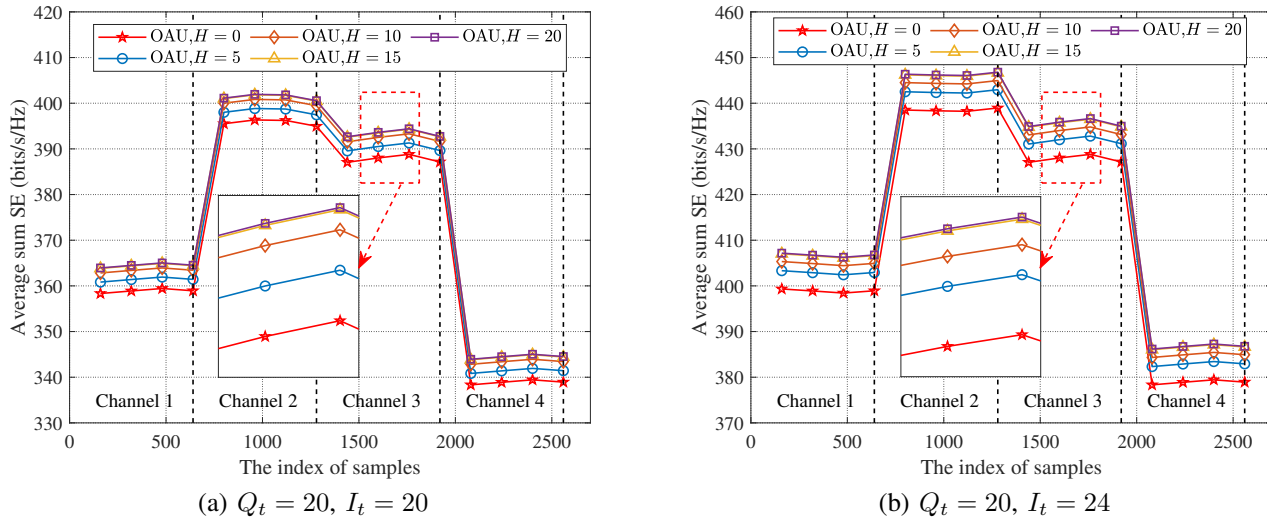


Fig. 6: Average sum SE of the proposed OAU algorithm for varying iterations H .

TABLE II: Average computation time of the proposed OAU algorithm for varying iterations H .

Algorithms	$Q_t = 20, I_t = 20$	$Q_t = 20, I_t = 24$
OAU, $H = 0$	0.58ms	0.71ms
OAU, $H = 5$	0.65ms	0.79ms
OAU, $H = 10$	0.72ms	0.88ms
OAU, $H = 15$	0.78ms	0.95ms
OAU, $H = 20$	0.84ms	1.04ms

insufficient iterations. Compared to WMMSE and L-WMMSE, Edge-GNN and SUNet reduce the average computation time by utilizing GNNs and CNNs to improve the computational efficiency, respectively, but they are designed in a fixed channel distribution configuration. When encountering the varying channels, the average sum SE of Edge-GNN and SUNet is degraded, since the deep learning assumption that the training and the inference stages have the same distribution for better generalization performance is violated. On the contrary, in addition to utilizing convolution units to improve the computational efficiency, HGNet designs the high-generalization beamforming module $\mathcal{G}(\cdot, \theta_l)$ to extract the valuable features for the varying channels, which effectively improves the sum SE performance of the varying channels. Consequently, HGNet achieves a higher sum SE with a computation time of less than 1ms.

C. Experimental Results for OAU Algorithm

To verify the effectiveness of the proposed OAU algorithm on the varying channels and the different numbers of APs and users, the average sum SE and computation time for varying iterations H are shown in Fig.6 and Table II, respectively. When the number of iterations H is set to 0, the proposed OAU algorithm is not applied to update the parameters of

HGNet. This is used as a comparative baseline for other different numbers of iterations H . As can be seen from Fig.6, the average sum SE gradually increases as H rises from 0 to 15, and does not increase significantly from 15 to 20. This improvement occurs because the proposed OAU algorithm iteratively updates the parameters of HGNet to improve the sum SE performance. As can be seen from Table II, with increasing the number of iterations H from 0 to 20, the average computation time becomes higher compared to the number of iterations $H = 0$. This is attributed to the fact that the proposed OAU algorithm consumes time to update the parameters of HGNet. In summary, the number of iterations of the proposed OAU algorithm can be selected as 15, which achieves a better sum SE performance and an average computation time of less than 1ms.

Fig.7 and Table III show the average sum SE and computation time of the proposed OAU algorithm with different numbers of update parameters of HGNet for varying iterations H , respectively. Specifically, the parameters in HGNet that can be updated by the proposed OAU algorithm is categorized into three groups: (1) BN layers, (2) CLs, and (3) a combination of BN layers and CLs. For simplicity, this paper refers to the approach of updating only the BN layers with fewer parameters (3%) as OAU algorithm. Since CLs contain more parameters of HGNet, updating only the parameters of CLs is termed as M-OAU algorithm. Updating both BN layers and CLs, which encompass all parameters of HGNet, is referred to as A-OAU algorithm. As shown in Fig.7 and Table III, when the number of iterations H for M-OAU and A-OAU algorithms is less than 15, their average sum SE is lower than that of OAU algorithm with $H = 15$, while their average computation time is significantly higher. This indicates that updating more parameters with fewer iterations does not necessarily outperform updating fewer parameters with more iterations, since training a larger number of parameters to a desired state requires sufficient iterations. As H gradually increases, both

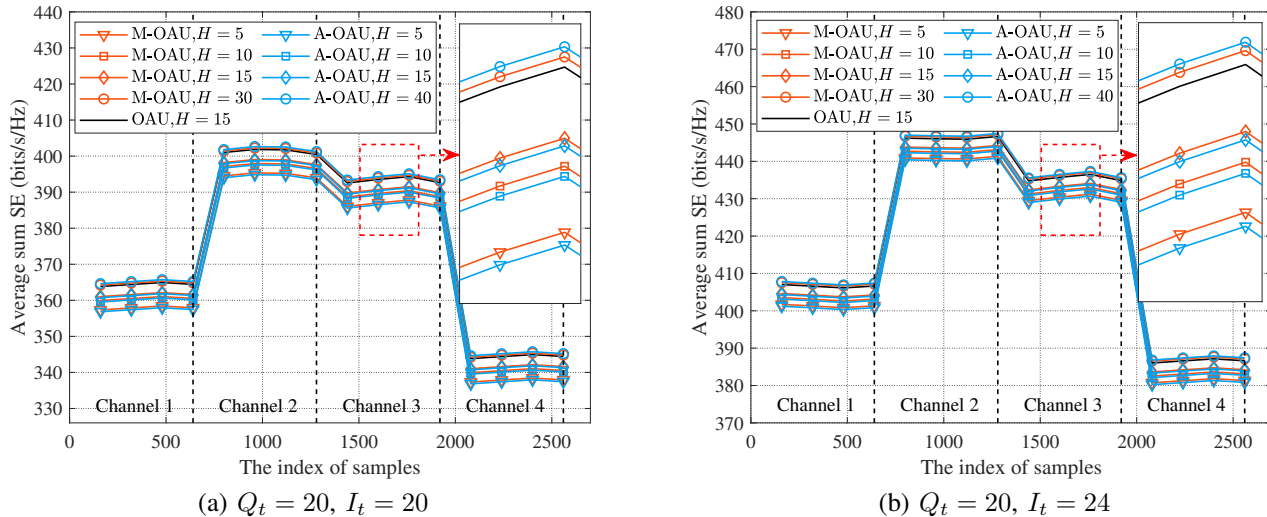


Fig. 7: Average sum SE of proposed OAU algorithm with different numbers of update parameters for varying iterations H .

TABLE III: Average computation time of the proposed OAU algorithm with different numbers of update parameters for varying iterations H .

Algorithms	$Q_t = 20, I_t = 20$	$Q_t = 20, I_t = 24$
M-OAU, $H = 5$	3.08ms	4.23ms
M-OAU, $H = 10$	5.61ms	7.76ms
M-OAU, $H = 15$	8.13ms	11.27ms
M-OAU, $H = 30$	15.69 ms	21.83ms
A-OAU, $H = 5$	3.15ms	4.31ms
A-OAU, $H = 10$	5.75ms	7.93ms
A-OAU, $H = 15$	8.33ms	11.51ms
A-OAU, $H = 40$	20.97ms	29.31ms
OAU, $H = 15$	0.78ms	0.95ms

M-OAU and A-OAU algorithms exhibit further improvements in the sum SE performance. For example, the average sum SE of M-OAU algorithm with $H = 30$ and A-OAU algorithm with $H = 40$ is higher than that of OAU algorithm with $H = 15$. However, the average computation time for M-OAU algorithm with $H = 30$ and A-OAU algorithm with $H = 40$ in the $Q_t = 20, I_t = 20$ and $Q_t = 20, I_t = 24$ scenarios is 15.69ms, 20.97ms, 21.83ms, 29.31ms, respectively. This poses a challenge in meeting real-time demands at the millisecond scale. In summary, the proposed OAU algorithm updating about 3% of the parameters of HGNet further improves the sum SE performance with an average computation time in the order of milliseconds.

VI. CONCLUSION

In this paper, HGNet with OAU algorithm is proposed to enable the online adaptive real-time beamforming design for dynamic wireless environments with the varying channels and the different numbers of APs and users in cell-free systems.

HGNet utilizes the residual structure of CNNs to adapt to the varying numbers of APs and users. Meanwhile, HGNet designs the high-generalization beamforming module to extract the valuable features of the varying channels for improving the generalization sum SE performance. Moreover, the OAU algorithm provides an online adaptive update mechanism for HGNet's parameters, enabling the online adaptive real-time beamforming design. Numerical results show that the proposed HGNet with OAU algorithm achieves a higher sum SE with a computation burden in the order of milliseconds, effectively meeting the demands of the real-time beamforming of cell-free systems in dynamic wireless environments.

APPENDIX A

PROOF OF PROPOSITION 3

To facilitate the analysis of the generalization error of $\mathcal{G}(\cdot, \theta_l)$ in HGNet, let $R_{\mathcal{T}_{in}}[\mathcal{G}, \mathcal{G}'] = \mathbb{E}_{x \sim \mathcal{T}_{in}}[\ell(\mathcal{G}(x, \theta_l), \mathcal{G}'(x, \theta'_l))]$ denote the generalization error risk of a pair $\mathcal{G}(\cdot, \theta_l)$ and $\mathcal{G}'(\cdot, \theta'_l)$ on the target domain \mathcal{T}_{in} , where $\ell(\cdot)$ denotes a error function. Note that the generalization error risk of $\mathcal{G}(\cdot, \theta_l)$ on \mathcal{T}_{in} is $R_{\mathcal{T}_{in}}[\mathcal{G}, 0] = \mathbb{E}_{x \sim \mathcal{T}_{in}}[\ell(\mathcal{G}(x, \theta_l), 0)]$, and $R_{\mathcal{T}_{in}}[\mathcal{G}] = R_{\mathcal{T}_{in}}[\mathcal{G}, 0]$ for simplification. Moreover, let $\mathcal{G}^*(\cdot, \theta_l^*)$ denote the ideal $\mathcal{G}(\cdot, \theta_l)$. By utilizing the triangular inequality, the following inequality can be obtained as

$$R_{\mathcal{T}_{in}}[\mathcal{G}] \leq R_{\mathcal{T}_{in}}[\mathcal{G}^*] + R_{\mathcal{T}_{in}}[\mathcal{G}^*, \mathcal{G}] + R_{\mathcal{T}_{in}}[\mathcal{G}^*, \mathcal{G}] - R_{\mathcal{T}_{in}}[\mathcal{G}^*, \mathcal{G}], \quad (25)$$

where $\overline{\mathcal{T}_{in}} = \sum_{t=1}^T \kappa_t \mathcal{S}_{tr}^t$ denotes a mixture of T varying channels closest to the target domain \mathcal{T}_{in} with $\sum_{t=1}^T \kappa_t = 1$.

By bringing $\overline{\mathcal{T}}_{\text{in}} = \sum_{t=1}^T \kappa_t \mathcal{S}_{\text{tr}}^t$ to Eq.(25),

$$R_{\overline{\mathcal{T}}_{\text{in}}}[\mathcal{G}] \leq R_{\overline{\mathcal{T}}_{\text{in}}}[\mathcal{G}^*] + \sum_{t=1}^T \kappa_t R_{\mathcal{S}_{\text{tr}}^t}[\mathcal{G}^*, \mathcal{G}] + \sum_{t=1}^T \kappa_t R_{\overline{\mathcal{T}}_{\text{in}}}[\mathcal{G}^*, \mathcal{G}] - \sum_{t=1}^T \kappa_t R_{\mathcal{S}_{\text{tr}}^t}[\mathcal{G}^*, \mathcal{G}], \quad (26)$$

Lemma 1: (Lemma 5.3 in [32]) With the previous definitions 1 and 2, the following inequality is held as

$$R_{\overline{\mathcal{T}}_{\text{in}}}[\mathcal{G}^*, \mathcal{G}] \leq R_{\mathcal{S}_{\text{tr}}^t}[\mathcal{G}^*, \mathcal{G}] + d_{\text{G-MMD}}(\mathcal{S}_{\text{tr}}^t, \overline{\mathcal{T}}_{\text{in}}).$$

Based on Lemma 1, Eq.(26) is rewritten as

$$R_{\overline{\mathcal{T}}_{\text{in}}}[\mathcal{G}] \leq R_{\overline{\mathcal{T}}_{\text{in}}}[\mathcal{G}^*] + \sum_{t=1}^T \kappa_t R_{\mathcal{S}_{\text{tr}}^t}[\mathcal{G}^*, \mathcal{G}] + \sum_{t=1}^T \kappa_t d_{\text{G-MMD}}(\mathcal{S}_{\text{tr}}^t, \overline{\mathcal{T}}_{\text{in}}), \quad (27)$$

where $\sum_{t=1}^T \kappa_t R_{\mathcal{S}_{\text{tr}}^t}[\mathcal{G}^*, \mathcal{G}]$ and $\sum_{t=1}^T \kappa_t d_{\text{G-MMD}}(\mathcal{S}_{\text{tr}}^t, \overline{\mathcal{T}}_{\text{in}})$ are applied to the triangular inequality, i.e.,

$$\sum_{t=1}^T \kappa_t R_{\mathcal{S}_{\text{tr}}^t}[\mathcal{G}^*, \mathcal{G}] \leq \sum_{t=1}^T \kappa_t R_{\mathcal{S}_{\text{tr}}^t}[\mathcal{G}^*] + \sum_{t=1}^T \kappa_t R_{\mathcal{S}_{\text{tr}}^t}[\mathcal{G}] \leq R_{\overline{\mathcal{T}}_{\text{in}}}[\mathcal{G}^*] + \sum_{t=1}^T \kappa_t R_{\mathcal{S}_{\text{tr}}^t}[\mathcal{G}], \quad (28)$$

$$\begin{aligned} & \sum_{t=1}^T \kappa_t d_{\text{G-MMD}}(\mathcal{S}_{\text{tr}}^t, \overline{\mathcal{T}}_{\text{in}}) \\ & \leq \sum_{t=1}^T \kappa_t d_{\text{G-MMD}}(\mathcal{S}_{\text{tr}}^t, \overline{\mathcal{T}}_{\text{in}}) + \sum_{t=1}^T \kappa_t d_{\text{G-MMD}}(\overline{\mathcal{T}}_{\text{in}}, \overline{\mathcal{T}}_{\text{in}}) \\ & \leq \sup_{t, t' \in \mathcal{T}} d_{\text{G-MMD}}(\mathcal{S}_{\text{tr}}^t, \mathcal{S}_{\text{tr}}^{t'}) + d_{\text{G-MMD}}(\overline{\mathcal{T}}_{\text{in}}, \overline{\mathcal{T}}_{\text{in}}). \end{aligned} \quad (29)$$

By bringing Eqs.(28) and (29) into Eq.(27),

$$R_{\overline{\mathcal{T}}_{\text{in}}}[\mathcal{G}] \leq \sup_{t, t' \in \mathcal{T}} d_{\text{G-MMD}}(\mathcal{S}_{\text{tr}}^t, \mathcal{S}_{\text{tr}}^{t'}) + d_{\text{G-MMD}}(\overline{\mathcal{T}}_{\text{in}}, \overline{\mathcal{T}}_{\text{in}}) + \varpi + \varrho, \quad (30)$$

where $\varpi = \sum_{t=1}^T \kappa_t R_{\mathcal{S}_{\text{tr}}^t}[\mathcal{G}]$ denotes the mixture weight of the generalization error for known source domains $\mathcal{S}_{\text{tr}}^t, t \in \mathcal{T}$. $\varrho = R_{\overline{\mathcal{T}}_{\text{in}}}[\mathcal{G}^*] + R_{\overline{\mathcal{T}}_{\text{in}}}[\mathcal{G}]$ denotes the combined error of ideal $\mathcal{G}^*(\cdot, \theta_l^*)$.

Lemma 2: (Theorem 29 in [39]) With the previous definitions 1 and 2, let $\widehat{\overline{\mathcal{T}}}_{\text{in}}$ and $\widehat{\mathcal{T}}_{\text{in}}$ denote the D data sampled from $\overline{\mathcal{T}}_{\text{in}}$ and \mathcal{T}_{in} , respectively. Then for all $\delta \in (0, 1)$, with probability at least $1 - \delta$, the following inequality is held as

$$\begin{aligned} d_{\text{G-MMD}}(\overline{\mathcal{T}}_{\text{in}}, \mathcal{T}_{\text{in}}) & \leq d_{\text{G-MMD}}(\widehat{\overline{\mathcal{T}}}_{\text{in}}, \widehat{\mathcal{T}}_{\text{in}}) + 2\sqrt{\frac{\log(\frac{2}{\delta})}{2D}} \\ & + \frac{2}{D} \left(\sum_{t=1}^T \kappa_t \mathbb{E} \left[\sqrt{\text{tr}(k_{\mathcal{S}_{\text{tr}}^t})} \right] + \mathbb{E} \left[\sqrt{\text{tr}(k_{\widehat{\mathcal{T}}_{\text{in}}})} \right] \right), \end{aligned}$$

where $k_{\mathcal{S}_{\text{tr}}^t}$ and $k_{\widehat{\mathcal{T}}_{\text{in}}}$ denote kernel functions computed on samples from $\mathcal{S}_{\text{tr}}^t$ and $\widehat{\mathcal{T}}_{\text{in}}$, respectively.

By bringing Lemma 2 into Eq.(30), we complete the proof of Proposition 3.

REFERENCES

- [1] G. Chen, Z. Wang, Q. Feng, S. Xiong, and Y. Huang, "High-generalization real-time beamforming design for dynamic wireless environments in cell-free systems," *To be published in 2025 IEEE Wireless Communications and Networking Conference (WCNC)*.
- [2] X. You, Y. Huang, S. Liu *et al.*, "Toward 6g TKμ extreme connectivity: Architecture, key technologies and experiments," *IEEE Wireless Communications*, vol. 30, no. 3, pp. 86–95, Jun. 2023.
- [3] N. Li and P. Fan, "Distributed cell-free massive mimo versus cellular massive mimo under ue hardware impairments," *Chinese Journal of Electronics*, vol. 33, no. 5, pp. 1274–1285, Sep. 2024.
- [4] G. Chen, S. He, Z. An, Y. Huang, and L. Yang, "A deep learning method: Qos-aware joint ap clustering and beamforming design for cell-free networks," *IEEE Transactions on Communications*, vol. 71, no. 12, pp. 7023–7038, Dec. 2023.
- [5] Q. Li, M. El-Hajjar, C. Xu, J. An, C. Yuen, and L. Hanzo, "Stacked intelligent metasurfaces for holographic mimo-aided cell-free networks," *IEEE Transactions on Communications*, vol. 72, no. 11, pp. 7139–7151, Nov. 2024.
- [6] Z. Wang, J. Zhang, H. Q. Ngo, B. Ai, and M. Debbah, "Uplink precoding design for cell-free massive mimo with iteratively weighted mmse," *IEEE Transactions on Communications*, vol. 71, no. 3, pp. 1646–1664, Mar. 2023.
- [7] W. Shi, Q. Wu, D. Wu, F. Shu, and J. Wang, "Joint transmit and reflective beamforming design for active irs-aided swipt systems," *Chinese Journal of Electronics*, vol. 33, no. 2, pp. 536–548, Mar. 2024.
- [8] Q. Shi, M. Razaviyayn, Z.-Q. Luo, and C. He, "An iteratively weighted mmse approach to distributed sum-utility maximization for a mimo interfering broadcast channel," *IEEE Transactions on Signal Processing*, vol. 59, no. 9, pp. 4331–4340, Sep. 2011.
- [9] Z. Liu, J. Zhang, Z. Liu, H. Du, Z. Wang, D. Niyato, M. Guizani, and B. Ai, "Cell-free xl-mimo meets multi-agent reinforcement learning: Architectures, challenges, and future directions," *IEEE Wireless Communications*, vol. 31, no. 4, pp. 155–162, Aug. 2024.
- [10] G. Chen, Z. Wang, H. Lin, Y. Huang, and L. Yang, "Computationally efficient unsupervised deep learning for robust joint ap clustering and beamforming design in cell-free systems," *IEEE Transactions on Wireless Communications*, 2025 (Early Access).
- [11] Y. Wang, Y. Li, Q. Shi, and Y.-C. Wu, "Learning cooperative beamforming with edge-update empowered graph neural networks," in *ICC 2023-IEEE International Conference on Communications*. IEEE, 2023, pp. 5111–5116.
- [12] G. Chen, Z. Wang, Y. Jia, Y. Huang, and L. Yang, "An efficient architecture search for scalable beamforming design in cell-free systems," *IEEE Transactions on Vehicular Technology*, vol. 73, no. 7, pp. 10241–10253, Jul. 2024.
- [13] W. Yu, Y. Shen, H. He, X. Yu, S. Song, J. Zhang, and K. B. Letaief, "An adaptive and robust deep learning framework for thz ultra-massive mimo channel estimation," *IEEE Journal of Selected Topics in Signal Processing*, vol. 17, no. 4, pp. 761–776, Jul. 2023.
- [14] J. Wang, C. Lan, C. Liu, Y. Ouyang, T. Qin, W. Lu, Y. Chen, W. Zeng, and P. S. Yu, "Generalizing to unseen domains: A survey on domain generalization," *IEEE Transactions on Knowledge and Data Engineering*, vol. 35, no. 8, pp. 8052–8072, Aug. 2023.
- [15] H. Sun, W. Pu, X. Fu, T.-H. Chang, and M. Hong, "Learning to continuously optimize wireless resource in a dynamic environment: A bilevel optimization perspective," *IEEE Transactions on Signal Processing*, vol. 70, pp. 1900–1917, Jan. 2022.
- [16] Q. Hou, M. Lee, G. Yu, and Y. Cai, "Meta-gating framework for fast and continuous resource optimization in dynamic wireless environments," *IEEE Transactions on Communications*, vol. 71, no. 9, pp. 5259–5273, Sep. 2023.
- [17] Q. Luo, Z. Han, and B. Di, "Meta-critic reinforcement learning for intelligent omnidirectional surface assisted multi-user communications," *IEEE Transactions on Wireless Communications*, vol. 23, no. 8, pp. 9085–9098, Aug. 2024.
- [18] A. AlAmmouri, H. ElSawy, A. Sultan-Salem, M. Di Renzo, and M.-S. Alouini, "Modeling cellular networks in fading environments with dominant specular components," in *2016 IEEE International Conference on Communications (ICC)*, 2016, pp. 1–7.
- [19] B. V. Philip, T. Alpcan, J. Jin, and M. Palaniswami, "Distributed real-time iot for autonomous vehicles," *IEEE Transactions on Industrial Informatics*, vol. 15, no. 2, pp. 1131–1140, Feb. 2019.
- [20] X. You, Y. Huang, C. Zhang, J. Wang, H. Yin, and H. Wu, "When ai meets sustainable 6g," *Science China Information Sciences*, vol. 68, no. 1, p. 110301, 2025.

- [21] E. Björnson and L. Sanguinetti, "Scalable cell-free massive mimo systems," *IEEE Transactions on Communications*, vol. 68, no. 7, pp. 4247–4261, Jul. 2020.
- [22] J. Fu, P. Zhu, J. Li, Y. Wang, and X. You, "Beamforming design in short-packet transmission for urllc in cell-free massive mimo system," *IEEE Systems Journal*, vol. 17, no. 3, pp. 4715–4724, Sep. 2023.
- [23] M. Hasan, S. Das, and M. N. T. Akhand, "Estimating traffic density on roads using convolutional neural network with batch normalization," in *2021 5th International Conference on Electrical Engineering and Information Communication Technology*. IEEE, 2021, pp. 1–6.
- [24] J. Zhang, C. Shen, H. Su, M. T. Arafat, and G. Qu, "Voltage over-scaling-based lightweight authentication for iot security," *IEEE Transactions on Computers*, vol. 71, no. 2, pp. 323–336, Feb. 2022.
- [25] Y. Ganin and V. Lempitsky, "Unsupervised domain adaptation by back-propagation," in *International conference on machine learning*. PMLR, 2015, pp. 1180–1189.
- [26] A. Shrikumar, P. Greenside, and A. Kundaje, "Learning important features through propagating activation differences," in *International conference on machine learning*. PMLR, 2017, pp. 3145–3153.
- [27] P. S. Efraimidis and P. G. Spirakis, "Weighted random sampling with a reservoir," *Information processing letters*, vol. 97, no. 5, pp. 181–185, Mar. 2006.
- [28] K. He, X. Zhang, S. Ren, and J. Sun, "Deep residual learning for image recognition," in *Proceedings of the IEEE conference on computer vision and pattern recognition*, 2016, pp. 770–778.
- [29] L. Pellaco, M. Bengtsson, and J. Jaldén, "Deep weighted mmse downlink beamforming," in *ICASSP 2021-2021 IEEE International Conference on Acoustics, Speech and Signal Processing (ICASSP)*. IEEE, 2021, pp. 4915–4919.
- [30] S. He, S. Xiong, Z. An, W. Zhang, Y. Huang, and Y. Zhang, "An unsupervised deep unrolling framework for constrained optimization problems in wireless networks," *IEEE Transactions on Wireless Communications*, vol. 21, no. 10, pp. 8552–8564, Oct. 2022.
- [31] Z. Fan, Q. Xu, C. Jiang, and S. X. Ding, "Weighted quantile discrepancy-based deep domain adaptation network for intelligent fault diagnosis," *Knowledge-Based Systems*, vol. 240, p. 108149, Mar. 2022.
- [32] I. Redko, E. Morvant, A. Habrard, M. Sebban, and Y. Bennani, *Advances in domain adaptation theory*. Elsevier, 2019.
- [33] A. Ma, J. Li, K. Lu, L. Zhu, and H. T. Shen, "Adversarial entropy optimization for unsupervised domain adaptation," *IEEE Transactions on Neural Networks and Learning Systems*, vol. 33, no. 11, pp. 6263–6274, Nov. 2022.
- [34] L. Sanguinetti, E. Björnson, and J. Hoydis, "Toward massive mimo 2.0: Understanding spatial correlation, interference suppression, and pilot contamination," *IEEE Transactions on Communications*, vol. 68, no. 1, pp. 232–257, Jan. 2019.
- [35] Y. He, Y. Cai, H. Mao, and G. Yu, "Ris-assisted communication radar coexistence: Joint beamforming design and analysis," *IEEE Journal on Selected Areas in Communications*, vol. 40, no. 7, pp. 2131–2145, Jul. 2022.
- [36] P. Higo Thaian da Silva, R. M. Duarte, H. S. Silva, M. S. Alencar, and W. J. L. De Queiroz, "Evaluation of cell-free millimeter-wave massive mimo systems based on site-specific ray tracing simulations," *IEEE Access*, vol. 10, pp. 82 092–82 105, 2022.
- [37] S. Sesia, I. Toufik, and M. Baker, "Lte-the umts long term evolution: From theory to practice. john wiley & sons, ltd," 2009.
- [38] S. E. Hajri, M. Assaad, and M. Larrañaga, "Enhancing massive mimo: A new approach for uplink training based on heterogeneous coherence times," in *2018 25th International Conference on Telecommunications (ICT)*. IEEE, 2018, pp. 361–366.
- [39] L. Song, "Learning via hilbert space embedding of distributions," *University of Sydney (2008)*, vol. 17, 2008.



Guanghai Chen (Graduate Student Member, IEEE) received the M.S. degree in the information and communication engineering from Chongqing University, Chongqing, China, in 2021. He is currently pursuing the Ph.D. degree in the information and communication engineering with the School of Information Science and Engineering, Southeast University. His research interests focus on intelligent wireless communications.



Zheng Wang (Senior Member, IEEE) received the B.S. degree in electronic and information engineering from Nanjing University of Aeronautics and Astronautics, Nanjing, China, in 2009, and the M.S. degree in communications from University of Manchester, Manchester, U.K., in 2010. He received the Ph.D degree in communication engineering from Imperial College London, UK, in 2015.

Since 2021, he has been an Associate Professor in the School of Information and Engineering, Southeast University (SEU), Nanjing, China. From 2015 to 2016 he served as a Research Associate at Imperial College London, UK. From 2016 to 2017 he was a senior engineer with Radio Access Network R&D division, Huawei Technologies Co.. From 2017 to 2020 he was an Associate Professor at the College of Electronic and Information Engineering, Nanjing University of Aeronautics and Astronautics (NUAA), Nanjing, China. His current research interests include massive MIMO systems, machine learning and data analytics over wireless networks, and lattice theory for wireless communications.



Hongxin Lin received the B.S. and M.S. degrees from Huaqiao University, Xiamen, China, in 2013 and 2016, respectively, and the Ph.D. degree from Southeast University, Nanjing, China, in June 2022. Since August 2022, he has been conducting post-doctoral research at the Purple Mountain Laboratories. His research interests include wireless communication technologies, such as millimeter wave communication, satellite communication, physical-layer security, massive MIMO cell-free networks, and URLLC.



Pengguang Du (Graduate Student Member, IEEE) received the B.Eng. degree in communication engineering from Jilin University, Changchun, China, in 2021. And he is currently pursuing the Ph.D. degree in information and communication engineering with the School of Information Science and Engineering, Southeast University, Nanjing, China. His research interests mainly focus on massive MIMO channel acquisition and intelligent wireless communications.



Yongming Huang (Fellow, IEEE) received the B.S. and M.S. degrees from Nanjing University, Nanjing, China, in 2000 and 2003, respectively, and the Ph.D. degree in electrical engineering from Southeast University, Nanjing, in 2007.

Since March 2007 he has been a faculty in the School of Information Science and Engineering, Southeast University, China, where he is currently a full professor. He has also been the Director of the Pervasive Communication Research Center, Purple Mountain Laboratories, since 2019. During 2008-2009, Dr. Huang visited the Signal Processing Lab, Royal Institute of Technology (KTH), Stockholm, Sweden. His current research interests include intelligent 5G/6G mobile communications and millimeter wave wireless communications. He has published over 200 peer-reviewed papers, hold over 80 invention patents. He submitted around 20 technical contributions to IEEE standards, and was awarded a certificate of appreciation for outstanding contribution to the development of IEEE standard 802.11aj. He served as an Associate Editor for the IEEE Transactions on Signal Processing and a Guest Editor for the IEEE Journal Selected Areas in Communications. He is currently an Editor-at-Large for the IEEE Open Journal of the Communications Society and an Associate Editor for the IEEE Wireless Communications Letters.